Mechanisms underlying the cooperation between loss of epithelial polarity and Notch signaling during neoplastic growth in *Drosophila*

Rémi Logeay[1], Charles Géminard[1], Patrice Lassus[2], Diala Kantar[1], Lisa Héron-Milhavet[1], Bettina Fischer[3], Sarah J. Bray[4], Jacques Colinge[1], and Alexandre Djiane[1]*

[1] IRCM, Inserm, Univ Montpellier, ICM, Montpellier, France

[2] IRCM, Inserm, Univ Montpellier, ICM, CNRS, Montpellier, France

[3] Dept. of Genetics, University of Cambridge, Cambridge, United Kingdom

[4] Dept. of Physiology Development and Neuroscience, University of Cambridge, Cambridge, United Kingdom

*Author for correspondence: IRCM, Inserm U1194
208, rue des Apothicaires
34298 Montpellier, Cedex, France
tel: +33 (0) 411 283 157
email: alexandre.djiane@inserm.fr

KEY WORDS:

Notch signaling, *Drosophila*, epithelial polarity, neoplasia

SUMMARY

Aggressive neoplastic growth can be initiated by a limited number of genetic alterations, such as the well-established cooperation between loss of cell architecture and hyperactive signaling pathways. However, our understanding of how these different alterations interact and influence each other remains very incomplete. Using *Drosophila* paradigms of imaginal wing disc epithelial growth, we have monitored the changes in Notch pathway activity according to the polarity status of cells and show that epithelial polarity changes directly impact the transcriptional output of the Notch pathway. Importantly, we show that this Notch pathway redirection is not mediated by a redeployment of Su(H), the Notch dedicated transcription factor, but relies on the cooperation with a combination of oncogenic transcription factors. Our work highlights in particular the role of the PAR domain containing bZIP transcription factor and Notch direct target Pdp1 for neoplastic growth.

39 **INTRODUCTION**

40 Epithelial cells represent the basic unit of many organs. They are polarized along an
41 apico-basal (A/B) axis, a feature critical for many aspects of their biology. A/B polarity
42 is controlled by the asymmetric segregation of highly conserved protein complexes
43 such as the Scrib/Dlg/Lgl complex (Bilder et al., 2003; Coopman and Djiane, 2016; St
44 Johnston and Ahringer, 2010). The far-reaching effects of A/B polarity is epitomized
45 by the observation that many tumors of epithelial origin exhibit impaired polarity, and
46 that several viral oncoproteins target polarity complexes (Banks et al., 2012; Huang and
47 Muthuswamy, 2010).

48 Studies in human cell lines and in animal models have also suggested a contributing
49 role of polarity alterations to tumor formation. For instance, mutations in the baso-
50 lateral determinant *SCRIB1* have been shown to control proliferation and invasion in
51 MCF-10A human mammary cells (Cordenonsi et al., 2011). Similarly in *Drosophila,*
52 *scrib*, *dlg* or *lgl* mutations, result in multilayered overgrowth of larval epithelial
53 imaginal discs (Bilder et al., 2003; Bunker et al., 2015). However, this uncontrolled
54 growth is at least partly achieved because larvae exhibiting *scrib* mutations fail to
55 undergo proper metamorphosis and imaginal discs grow for an extended period. Indeed,
56 *scrib* mutant cells actually grow slower than wild-type cells and are eliminated by wild-
57 type neighbors (Cordero et al., 2010; Igaki et al., 2009, 2006; Ohsawa et al., 2011).
58 Interestingly, this is reversed when additional mutations are introduced, such as
59 overexpression of the BTB/POZ chromatin remodelers Abrupt or Chinmo (Doggett et
60 al., 2015; Turkel et al., 2013) or the constitutive activation of signaling pathways (e.g.
61 Ras or Notch), converting *scrib* mutant cells into aggressive, invasive and
62 hyperproliferative cells (Brumby and Richardson, 2003; Pagliarini and Xu, 2003).
63 Similar observations have been reported in mouse, where Notch or Ras activation and

64 *Par3* depletion cooperate to generate aggressive neoplasms in mouse mammary glands
65 (McCaffrey et al., 2012; Xue et al., 2013).

66 The Notch pathway is a highly conserved cell-signaling pathway mis-regulated in
67 several cancers (Ntziachristos et al., 2014; Ranganathan et al., 2011). Upon activation,
68 Notch receptors undergo two proteolytic cleavages to release their intra-cellular domain
69 or NICD, which enters the nucleus, binds to the Notch pathway specific transcription
70 factor CSL (Rbpj in mammals; Suppressor of Hairless, Su(H) in *Drosophila*), and
71 converts it from a repressor to an activator to turn on the transcription of specific target
72 genes (Bray, 2016). These Notch direct target genes differ depending on cell type and
73 account for the variety of outcomes triggered by Notch activity. Increased Notch
74 activity has been associated with several epithelial cancers such as non-small-cell lung
75 carcinomas (Maraver et al., 2012; Ntziachristos et al., 2014), but in animal models, the
76 sole increase in Notch activity either promotes differentiation or only results in benign
77 over-proliferation (hyperplasia) (Brumby and Richardson, 2003; Djiane et al., 2013;
78 Fre et al., 2005; Ho et al., 2015; McCaffrey et al., 2012). However, as mentioned
79 previously, Notch pathway activation cooperates with loss of polarity to generate
80 invasive neoplasms (Brumby and Richardson, 2003; Ho et al., 2015; McCaffrey et al.,
81 2012; Pagliarini and Xu, 2003).

82 So, while the cooperation between loss of cell architecture and hyperactive signaling
83 pathways is well established, the underlying mechanisms remain poorly understood. It
84 could merely reflect an additive effect where the consequences of both events combine.
85 Alternatively, it could indicate a more profound integration within epithelial cells where
86 these two events impact on each other to generate unique new behaviors. Using
87 *Drosophila* paradigms of imaginal wing disc epithelial growth, we have monitored the
88 changes in Notch pathway activity according to the polarity status of cells and show

89 that epithelial polarity changes directly impact the transcriptional output of the Notch
90 pathway. We further provide evidence that this Notch redirection is not mediated by
91 new genomic binding regions for Su(H), but relies on the cooperation with Su(H) of a
92 combination of transcription factors, such as Stat and basic leucine zipper (bZIP),
93 whose activity is triggered in response to JNK signaling during polarity loss, extending
94 earlier reports on the cooperation between oncogenic Ras and polarity loss (Atkins et
95 al., 2016; Davie et al., 2015; Külshammer et al., 2015; Uhlirova and Bohmann, 2006).
96 Our work highlights in particular the role of the PAR domain containing bZIP
97 transcription factor Pdp1 for Notch-driven neoplastic growth.
98

RESULTS

Notch activation and scrib mutation cooperate to promote neoplastic growth

In order to gain insights into the mechanisms underlying neoplastic growth, we first characterized the effects of Notch activation and *scrib* mutation mediated epithelial polarity impairment on wing disc growth. Using precisely controlled *Drosophila* larvae culture conditions (crowding and timing), we compared the phenotypes of wild-type (WT), Nicd overexpressing (N), *scrib* mutant (S), and Nicd overexpressing and *scrib* mutant (NS) 3rd instar wing imaginal discs at 6 days after egg laying at 25C. These different paradigms are shown in Figure 1A-D. For clarity, in all figures N will be shown in green, S in red, and NS in blue. Reproducing our previous observations (Djiane et al., 2013), N discs overgrew compared to WT, but remained as monolayered epithelia with properly localized E-Cadherin-based adherens junctions, and represent a paradigm of hyperplastic-like growth (Fig. 1A&B). S discs were smaller than WT, but grew as unstratified mass of cells with weak uniform E-Cadherin (E-Cad). These discs however showed an extensive expression of the JNK signaling target Mmp1 (Fig. 1C), a metallo-protease implicated in the digestion of the extracellular matrix, indicative that *scrib*- cells activate JNK signaling and are prone to invasiveness (Igaki et al., 2006; Uhlirova and Bohmann, 2006). It is noteworthy that S larvae did not pupariate and if left to grow for longer, the S discs ultimately developed as massive overgrowths with very disrupted epithelial polarity, that invaded and fused with neighboring tissues such as other discs (Bilder et al., 2003). Strikingly, NS discs combined aspects of N and S discs. They were overgrown like N discs, but also expressed low levels of E-Cad and high levels of Mmp1 like S discs (Fig. 1D). These discs grew as multilayered tissues and were able to invade the surrounding tissues such as haltere discs, and represent therefore a paradigm for neoplastic-like growth.

Neoplastic and hyperplastic discs have different transcriptomes

The context of the *scribble* mutation converts the Notch-based *Drosophila* wing disc hyperplasia into a paradigm of neoplastic growth. While the cooperation between activated Ras and *scrib* mutations has been studied extensively, mainly in the eye imaginal disc (Atkins et al., 2016; Cordero et al., 2010; Davie et al., 2015; Igaki et al.,

132 2009; Katheder et al., 2017; Pagliarini and Xu, 2003; Toggweiler et al., 2016; Wu et
133 al., 2010), less attention has been given to the cooperation between polarity loss and
134 other activated pathways, such as Notch or Hedgehog (Brumby and Richardson, 2003;
135 Pagliarini and Xu, 2003), preventing an evaluation of how general the studies on Ras
136 signaling are to neoplasia development.
137
138 First, we compared the RNA-Seq transcriptomes of the different genetic conditions, to
139 identify the differently expressed genes in N, S, and NS compared to WT controls
140 (using DESeq with adjusted p-value for multiple testing <0.05; Fig. 1E&F and
141 Supplemental Table S1; (Anders and Huber, 2010). The numbers were broadly similar
142 in the different conditions, N (503 up; 663 dw), S (757 up; 1029 dw), and NS (1003 up;
143 991 dw). Semi-quantitative qRT-PCR validated in a subset of genes the transcriptional
144 changes. For instance, *E2f1*, *Sdr*, and *mxc*, were activated only in N discs, while *Act87E*
145 and *Wnt10*, were activated only in NS. In addition, *Ets21C*, *ftz-f1*, and *Atf3* were up-
146 regulated in all conditions (Supplemental Fig. S1A). Comparing these data with
147 previously published transcriptomes on similar or related genetic backgrounds revealed
148 significant overlap, validating our experimental approaches. For instance, 174/503 up-
149 regulated, and 285/663 down-regulated genes in N were also detected in our previous
150 analysis using dual color differential expression arrays (significant overlap p=1.11e-
151 273, hypergeometric test; (Djiane et al., 2013). Similarly, 676/757 up-regulated genes
152 in S were identified in a previous analysis of *scrib* depleted discs (significant overlap
153 p=4.90e-193; (Bunker et al., 2015).
154
155 GO term analysis (p-value < 0.05) confirmed that, as expected from their genetic
156 composition, the N and NS transcriptomes had over-representation for genes in the
157 Notch signaling pathway (GO:0007219) while the NS and S transcriptomes for genes
158 affected by changes in A/B polarity (GO:0045197; GO0019991) (Fig. 1G). This
159 analysis revealed potential common behaviors shared by N and NS, in particular signs
160 of increased proliferation, consistent with the overgrowth phenotypes (e.g. "mitotic
161 cytokinesis" and "mitotic spindle organization"; GO:0000281; GO:0007052), or
162 behaviors shared between NS and S, such as those related to cell migration (e.g. "border
163 follicle cell migration"; GO:0007298) or cellular stress (e.g. "response to starvation"
164 GO:0042594; "response to endoplasmic reticulum stress" GO:0034976) (Fig. 1G).

165 Notably several GO categories were enriched specifically in NS, including "mitotic
166 G1/G2 DNA damage checkpoint" (GO:0031571/GO:0007095), or gluthatione
167 metabolic process (GO:0006749). These results argue that the combined Notch
168 activation and polarity loss promoted the emergence of new cell behaviors and
169 responses, in particular related to DNA damage responses (Fig. 1G).
170
171
172 ***Hyperplasia and neoplasia harbor different Notch direct target networks***
173 The transcriptomic changes revealed that NS encompassed not only additive N and S
174 features but also the emergence of new behaviors. This raises the question of how the
175 defects in *Notch* and in *scrib* cooperate to produce these transcriptional consequences.
176 One particularly critical aspect is how the Notch pathway is affected by the *scrib*
177 mutation. Many signaling pathways, such as Ras, branch and act through several
178 transcription factors and/or combine nuclear and cytoplasmic responses, making the
179 analysis of how they are affected by the *scrib* mutation complicated. Since the Notch
180 pathway is extremely direct and since the major, if not unique, output of Notch
181 signaling is transcriptional activation (Bray, 2016), it offers a unique opportunity to
182 investigate how the *scrib* mutation could potentially affect Notch signaling in the NS
183 cooperation. We thus decided to monitor the genes directly activated by Notch and
184 study whether the Notch direct programme (Notch Direct Targets, NDTs) is affected
185 by the *scrib* mutation.
186 Genes that are directly regulated by Notch (NDTs) should have the transcription
187 complex, containing Su(H) bound at their regulatory regions (Djiane et al., 2013). To
188 identify potential NDTs in N and NS, we thus monitored the genomic regions occupied
189 by the Su(H) transcription factor by genome-wide Chromatin Immuno-Precipitation
190 (ChIP) (Fig. 2A; Supplemental Table S2). These overlapped significantly with our
191 previous analysis of Notch induced overgrowth, suggesting that we have captured all
192 the robust regions of Su(H) enrichment.
193
194 Strikingly, there was a strong overlap in the Su(H) bound regions between N and NS
195 conditions: almost all NS Su(H) peaks (416 out of a total of 464) overlap with peaks
196 present in N discs. This implies that the vast majority of Su(H) binding in NS were also
197 present in N (Fig. 2C & S1C). The overlap was also important between N and S peaks

198 (447/554 S peaks overlapping with N peaks; Fig. 2C & S1C). These results suggests
199 that in NS neoplastic discs, a minority of Su(H) peaks represent new binding regions
200 compared to hyperplastic N discs, and that the new NS behaviors are not the
201 consequence of general redistribution of the Notch specific transcription factor Su(H).
202
203 In order to estimate the programs specifically activated by Notch in N and NS, we then
204 intersected the transcriptomic data with the Su(H) ChIP data, considering that
205 upregulated genes located within 20kb of a Su(H) peak were likely NDTs. Using this
206 approach, we identified similar numbers of NDTs in N (176) and NS (174) (Fig. 2A&B,
207 Supplemental Table S3). Again, there was substantial overlap with previous data, with
208 64/176 NDTs in the N condition being identified in our previous study (significant
209 overlap p=5.89e-96, hypergeometric test; (Djiane et al., 2013). When the N and NS
210 scenarios were compared, 68 genes were common to both and thus represent core NDTs
211 in the wing disc overgrowth. However, a significant proportion of NDTs appeared
212 specific for each condition: 108 for N, 106 for NS. Amongst the 106 NS-specific NDTs,
213 23 were also NDTs in S. Indeed, affecting only polarity with the *scrib* mutation already
214 alters the Notch programme (123 NDTs in S). But the difference between N and NS
215 cannot just be explained by this S contribution as it concerns only 23 NDTs, and taking
216 all comparisons into account, 83 genes appear as true NS-specific NDTs (Fig. 2B).
217 Only a minority were associated with new Su(H) binding regions: around the *87E* locus
218 (*yellow-e3, yellow-e, Ir87a,* and *Act87E*), and the *94A* locus (*CG18596, CG7059,*
219 *CG13857,* and *CG13850*), but also next to the *vito*, *cdi*, and *REG* genes (see
220 Supplemental Table S3).
221 These results indicate that while a core Notch response can be identified in overgrowing
222 wing discs (68 genes; Fig. 2B), the loss of polarity affected the direct transcriptional
223 output of the Notch signaling pathway: 108 NDTs specific to N were lost, while 83
224 NDTs specific to NS were gained. Importantly these changes in the Notch program are
225 only marginally mediated by a redeployment of the Su(H) transcription factor: 11/83
226 NS NDTs correspond to NS-specific Su(H) enrichment. Interestingly, amongst the 83
227 NS-specific NDTs are p53, His2Av, and the Tip60 complex component Act87E (Kusch
228 et al., 2004), which have all been linked to DNA damage response and could therefore
229 account for the NS emergent behaviors identified in the GO term analysis (Fig. 1G).
230

231

232 ***Neoplastic overgrowth is not mediated by the new NS-specific Su(H) regions***

233 Using the NDT datasets, we sought to identify the factors that are required for the
234 transition from N hyperplastic to NS neoplastic growth.

235 First, we decided to investigate the contribution of the DNA damage response. Indeed
236 several NS-specific NDTs are implicated in DNA damage response and the GO analysis
237 highlighted categories specific to NS related to "response to oxidative stress"
238 (GO:0006979), "cellular response to gamma radiation" (GO:0071480), and "DNA
239 damage checkpoints" (GO:0031571/0007095). We thus asked whether interfering with
240 such pathways could block the growth and invasiveness of NS tissues. To perform these
241 genetic tests, we generated a stable fly line which overexpressed *Nicd* and *scribRNAi*
242 together with a *GFP* marker under the *Bx-Gal4* driver (driving expression in the pouch
243 of the larval wing discs; *Bx>NS*), and monitored the size of the overgrowth (GFP
244 positive tissue), and its invasiveness potential (Mmp1 expressing cells; Fig. 4A).

245 Blocking the oxidative stress response by overexpressing the Reactive Oxygen Species
246 (ROS) sponge CAT and SOD, did not have any significant effect on the NS overgrowth
247 or the expression of Mmp1 (Fig. 4E&F). Similarly, expression of RNAi or dominant
248 negative forms of the severe DNA damage major effector and NS specific NDT *p53*
249 could not modify the NS overgrowth phenotype (Fig. 4E&F). While we cannot exclude
250 that the tools used here were not strong enough, these results suggest that even though
251 activated in NS tissues, oxidative stress and p53-mediated DNA damage responses
252 were either not required to fuel NS growth, or that they could compensate for each other
253 converging ultimately on an as yet unidentified core response promoting NS growth.

254

255 Second, we turned our attention to the NS specific NDTs associated with unique Su(H)
256 binding. Indeed, even though the emergence of new Su(H) binding is not the main
257 mechanism driving the NS-specific Notch programme, it remains possible that these
258 loci and the genes associated are functionally important for the NS neoplastic behavior.
259 We thus asked whether interfering with these 11 specific NS NDTs could block the
260 growth and invasiveness. Knocking down by RNAi the expression of the different
261 genes associated with the *87E* locus (*yellow-e3, yellow-e, Ir87a,* and *Act87E*), and with
262 the *94A* locus (*CG18596, CG7059, CG13857,* and *CG13850*) did not have any
263 significant effect on the NS overgrowth. Similarly, we could not detect any change in

264 NS tumor overgrowth after RNAi-mediated knock-down for *cdi*, *REG,* and *vito* (data
265 not shown). It should be noted however that for several genes only one RNAi could be
266 tested with the potential caveat of insufficient knock-down efficiencies (Xia et al.,
267 2021). However, our results suggest that these NS-specific Su(H) NDTs are not
268 required, at least individually, for NS overgrowth. But even though not strictly required,
269 their overexpression, might still contribute, redundantly with other factors, to the
270 overall NS neoplastic behaviors. Amongst these particular NS NDTs, *Act87E,*
271 associated with the new Su(H) peak at locus *87E* (Fig. 2D) was the most robustly up-
272 regulated in NS (see Supplemental Table S1 & Fig. S1A). When overexpressed in wild-
273 type wing disc, or in combination with activated Notch, Act87E led to robust expression
274 of the metalloprotease and JNK target Mmp1, and cell delamination. Act87E also
275 induced robust expression of the effector caspase Dcp-1 caspase (Supplemental Fig.
276 S2). Act87E, might thus represent a stress gene activated in NS initiating cell
277 delamination and ultimately cell death, but whose role is not necessary and/or
278 redundant with other NS-activated genes.
279
280
281 ***Identification of the transcriptional networks in the different growth paradigms***
282 Taken together our results indicate that even though the *scrib* mutation was able to
283 change the transcriptional output of the Notch pathway, the difference between N and
284 NS is not due to a redeployment of Su(H) to activate new NS-specific genes. Other
285 factors brought upon the *scrib* mutation must thus influence gene expression.
286 We thus sought to identify transcriptional factors that could account for the cooperation
287 between Notch and polarity loss. We used the iRegulon software to identify the
288 transcription factors likely co-regulating the genes identified in N, S, or NS. Previous
289 usage of iRegulon on *RasV12/scrib-* overgrown 3rd instar larval discs, highlighted an
290 "oncogenic module" comprising of the Hippo pathway terminal effectors Yki/Sd, the
291 JNK pathway regulated AP-1 factors (in particular Atf3, Kay, and CEBPG), the
292 Jak/Stat pathway, Myc, Crp, and Ftz-F1, (Atkins et al., 2016; Davie et al., 2015;
293 Külshammer et al., 2015).
294
295 Implementing iRegulon on our step-wise Notch-based paradigms allowed us (i) to
296 identify transcriptional modules unique or shared between polarity loss only (S),

297 proliferation only (N), and proliferation plus invasiveness (NS), and (ii) to assess the
298 conservation of the "oncogenic module" identified previously with Ras in a Notch-
299 driven neoplastic paradigm. We performed these analyses feeding iRegulon either with
300 the lists of up-regulated genes in N, S, and NS (Fig. 3 & Supplemental Table S4) or
301 with the lists of NDTs (Fig. S3 & Supplemental Table S5). We decided to focus our
302 analyses on the up-regulated genes here since the overexpressed Nicd triggers
303 transcriptional activation (Bray, 2016) and down-regulated genes might thus represent
304 very indirect effects of the cooperation. Modules identified are presented as Venn
305 diagrams (Fig. 3&S3) highlighting the common and specific transcription factor
306 modules that were identified as likely master regulators of the transcriptional changes
307 in the different conditions. Feeding either up-regulated genes (Fig. 3) or NDTs (Fig.
308 S3) identified similar modules indicating that the Notch pathway condition-specific
309 transcription programs are mediated, at least in part, by transcription factors that
310 broadly affect the whole transcriptome. This is likely also true for other neoplastic
311 paradigms such as Ras, even though this remains to be established. Importantly,
312 iRegulon identified the Notch pathway dedicated transcription factor Su(H) in the N
313 and NS transcriptomes.
314
315 First, focusing on NS, which most resembles the *RasV12/scrib-* paradigms, our analysis
316 identified the same major nodes and oncogenic module as described previously:
317 - AP-1 basic Leucine Zipper factors related to stress kinase signaling
318 - Stat92E of the Jak/Stat pathway
319 - Ftz-F1 nuclear receptor
320 - basic Helix-Loop-Helix factors of the Myc family.
321 In NS transcriptome, we also identified a contribution of the E(spl) bHLH
322 transcriptional repressors. *E(spl)-HLH* genes are canonical Notch targets, and they are
323 robustly up-regulated in N and NS, in particular *E(spl)mγ-HLH*.
324
325 The iRegulon analyses also suggested that the AP-1 bZIP, and the Stat92E signatures
326 in NS are contributed by S, since they are also detected in the S transcriptomes, while
327 the Su(H) signature is contributed by N. Finally, iRegulon identified a signature for the
328 Polycomb chromatin silencers specifically in N. Such factors include Pho, a zinc finger
329 protein which binds to Polycomb Responsive Elements (PREs) and recruits Polycomb

330 complexes, and the three Polycomb Repressor Complex 1 components Psc, Su(z)2, and
331 l(3)73Ah. Recently, PRC1 has been associated with specific and unexpected
332 transcriptional activation at larval stages, raising the possibility that in N, such genes,
333 normally repressed at embryonic stages, become active (Loubiere et al., 2020).
334 However, the exact contribution of Polycomb factors, and whether they are actually
335 involved in gene activation upon Notch activation, or whether the "Polycomb" module
336 of iRegulon merely indicates gene de-repression, has not been addressed formally in
337 this study.
338
339
340 ***A polarity-loss oncogenic module***
341 In order to validate the functional relevance of the transcription factors identified in the
342 Notch-driven neoplastic growth, we then asked whether their depletion by RNAi could
343 alter the growth and invasiveness of the NS tissue, using the *Bx>NS* fly line described
344 previously. We first focused our analysis on the oncogenic module.
345
346 We confirmed earlier reports that blocking JNK activity by the overexpression of a JNK
347 dominant negative construct, strongly abolishes NS driven growth (GFP positive tissue
348 size; Fig. 4B&E) and invasiveness (Mmp1 expression; Fig. 4B&F). As shown in the
349 *RasV12/scrib-* paradigms, RNAi mediated knock-down of the Jak/Stat pathway
350 terminal transcription factor *stat92E*, and to a lesser extent *ftz-f1* (Atkins et al., 2016;
351 Davie et al., 2015; Külshammer et al., 2015; Toggweiler et al., 2016) strongly
352 suppressed both growth (GFP) and invasiveness (Mmp1; Fig. 4E&F). Unlike the
353 RasV12 models, we did not identify in the different iRegulon analyses of the N, S, and
354 NS transcriptomes, any particular enrichment for Sd/TEAD, the transcriptional factor
355 mediating the effect of Yki and of the Hippo pathway mediated growth in wing discs.
356 However, impairing Yki activity (through RNAi-mediated knock-down) strongly
357 suppressed NS neoplastic behaviors (Fig. 4C,E&F).
358
359 Taken together these results suggest that independently of the oncogenic driver, Ras or
360 Notch, relatively similar tumorous transcriptional networks (AP-1/Yki/Stat/Ftz-f1) are
361 put in place during their cooperation with polarity loss (Atkins et al., 2016; Davie et al.,
362 2015; Külshammer et al., 2015). Given that these nodes were also identified in the S

363 transcriptome, we suggest that they represent a polarity loss module cooperating with
364 oncogenic signaling pathways Ras or Notch, and likely other pathways such as Hh as
365 was initially reported (Brumby and Richardson, 2003).
366
367
368 ***The PAR domain containing transcription factor Pdp1 is required for neoplastic***
369 ***growth***
370 A striking feature of the iRegulon analyses was the NS/S JNK module, which contained
371 classic basic leucine zipper (bZIP) transcription factors such as Jun or Fos. These
372 factors are involved in complex homo and hetero-dimers mediating cellular responses
373 to different stresses such as DNA damage, oxidative stress… (Reinke et al., 2013), and
374 their binding specificities remain difficult to tease apart. Atf3 has recently been shown
375 to control the expression of genes involved in the maintenance of epithelial polarity,
376 and to be specifically activated in polarity deficient cells and required in the
377 *RasV12/scrib-* overgrowth models (Atkins et al., 2016; Donohoe et al., 2018).
378 Strikingly, amongst the different bZIP predicted by iRegulon to control the NS
379 transcriptome, *Pdp1* is a direct Notch target (common in N, S, and NS; Supplemental
380 Table S3 & Fig. S4A), raising the interesting prospect that Pdp1 could act as feed-
381 forward factor to promote neoplastic growth downstream of Notch.
382 Knocking down *Pdp1* using two independent RNAi lines, using the *Bx>NS* fly line, led
383 to a robust reduction of tissue growth (as measured by total GFP area; Fig. 4D&E), and
384 to a reduction in the intensity of Mmp1 staining (Fig. 4D&F). Pdp1 (the homologue of
385 Hepatic Leukemia Factor - HLF) has previously been linked to mitotic cell cycle and
386 growth (Reddy et al., 2006), and shown in the *RasV12/scrib-* paradigms to have only
387 modest effects on invasion, but none on growth. In the context of Notch (*Nicd/scrib-*),
388 the role of *Pdp1* appeared thus more essential, probably because *Pdp1* is a direct Notch
389 target. Furthermore, Pdp1 was also sufficient to induce cell delamination and spreading,
390 as evidenced by the scar left and broader width along the *Dpp-Gal4* stripe of Pdp1
391 overexpression (Fig. S4C). Taken together, these results highlight the important role of
392 Pdp1 in Notch-driven neoplasia.
393

394 **DISCUSSION**

395 In this study, using Notch-driven paradigms of epithelial overgrowth in *Drosophila*
396 wing discs, we describe the molecular mechanisms underlying the cooperation between
397 Notch and polarity loss during neoplasia. We show that epithelial polarity alterations
398 redirect the transcriptional outcome of the Notch signaling pathway, thus defining a
399 specific set of new neoplastic Notch direct targets. We further show that this redirection
400 occurs mainly on pre-existing Su(H) bound regions rather than new ones. Finally, we
401 show that similarly to what was previously described for Ras signaling (Atkins et al.,
402 2016; Davie et al., 2015), the cooperation between Notch signaling and polarity loss is
403 controlled by a "tumor transcriptional network" centered around the AP-1/Stat/Yki/Ftz-
404 f1 transcription factors, governing the implementation of this new neoplastic Notch
405 programme.

406

407 While cancer genomes exhibit multiple mutations in cancer cells, their functional
408 interactions remain difficult to monitor and model. Neoplastic tissues, generated upon
409 the combination of Notch pathway activation and polarity loss through *scrib* mutation,
410 experience many cellular stresses: DNA damage responses, but also ER and unfolded
411 protein response, starvation, or oxidative stresses. However, even though present, these
412 different stresses and in particular oxidative stress and DNA damage are not
413 individually necessary in the context of polarity loss as blocking them or the cellular
414 response they promote (CAT/SOD overexpression, or inhibition of p53) could not
415 significantly suppress the NS tumorous behaviors. These observations suggest that the
416 different stress pathways activated during polarity loss are either not required for
417 fueling growth (they are rather a consequence than a cause of neoplastic growth), or
418 might act "redundantly" to activate a common core response required for increased
419 growth.

420

421 While *Drosophila* and mouse models have demonstrated that overactive signaling
422 pathways cooperate with epithelial polarity impairment to generate neoplastic growth
423 (Brumby and Richardson, 2003; McCaffrey et al., 2012; Pagliarini and Xu, 2003; Xue
424 et al., 2013), the vast majority of studies seeking to understand the underlying
425 mechanisms, have focused primarily on the cooperation between activated RasV12 and
426 *scrib* mutants, especially in *Drosophila* (Atkins et al., 2016; Cordero et al., 2010; Davie

427 et al., 2015; Igaki et al., 2009; Katheder et al., 2017; Pagliarini and Xu, 2003;
428 Toggweiler et al., 2016; Wu et al., 2010). Importantly, the current study, investigating
429 the cooperation between Notch and polarity, shows that many observations made for
430 Ras can be extended to Notch, suggesting that the paradigms used are not a Ras
431 specificity but might represent a more general tumor growth paradigm.
432
433 But even though we could highlight the involvement of a core "oncogenic module"
434 (Atkins et al., 2016; Davie et al., 2015; Külshammer et al., 2015), there are specifics
435 that are likely oncogene specific. First, unlike what was reported for *RasV12/scrib-*
436 transcriptomes, Yki/Sd/TEAD modules were not found enriched in the different *Notch*
437 and *scrib-* transcriptomes. In the case of Ras, it was shown that Yki activity could
438 reprogram Ras by promoting the expression of the Ras pathway specific regulators
439 Capicua and Pointed to promote aggressive growth (Pascual et al., 2017). Both genes
440 were either unaffected (*capicua*) or downregulated (*pointed*) in NS Notch driven
441 neoplastic paradigm, suggesting that, even though Yki is clearly required (Fig. 4C),
442 changes in the expression of capicua and pointed are unlikely mediators here. These
443 differing results in the enrichment of Yki/Sd/TEAD motifs between Notch and Ras
444 transcriptomes in the context of polarity loss, might reflect the inhibitory effect Notch
445 has on Yki activity in the wing pouch, in part through the action of the *vestigial* (Djiane
446 et al., 2014). Furthermore, in NS transcriptome, we identified a contribution of the
447 E(spl) bHLH transcriptional repressors, canonical Notch targets (Bray, 2016), which
448 represents thus a Notch specificity. However, the fact that motifs for E(spl)-HLH
449 repressors are found in the up-regulated transcriptome of NS and not N could suggest
450 that in NS, the repressive ability of E(spl)-HLH factors is antagonized, further allowing
451 higher expression of Notch targets. More precisely, our previous work identified many
452 incoherent feed-forward loops in the N hyperplastic transcriptome, including through
453 the action of E(spl) repressors (Djiane et al., 2013), which might thus be resolved in
454 NS. It would be interesting to explore further the link between NS and E(spl)-HLH-
455 mediated repression, but due to the high redundancy between the seven E(spl)-HLH
456 factors (δ, γ, β, 3, 5, 7, 8) and Dpn, the requirement of E(spl)-HLH-mediated repression
457 in the Notch-driven neoplasia could not be formally tested.
458

459 While performing functional assays to identify the genes and processes required for NS
460 tumor growth, we could show that the Notch direct targets associated with "de-novo"
461 NS-specific Su(H) peaks were unlikely to be major contributors. We show however
462 that the bZIP PAR domain containing factor Pdp1 is required for NS tumor growth and
463 invasiveness. Su(H) is bound in the vicinity of Pdp1 in all wing discs set-ups and in
464 particular in N and NS, and Pdp1 represents a "core" Notch target activated in all
465 overgrowth conditions, albeit at higher levels in polarity deficient conditions (Fig.
466 S4A). Pdp1 is not only a Notch target, but also a Jak/Stat target, at least in the
467 developing eye, and canonical tandem Stat92E putative binding sites are found in its
468 second intron, although not overlapping with Su(H) binding which is found in its first
469 intron (Flaherty et al., 2009). Interestingly, Pdp1 is required for Stat92E
470 phosphorylation and efficient Jak/Stat signaling (Baeg et al., 2005), suggesting that
471 Notch might amplify Stat92E signaling during wing disc neoplastic growth, both
472 through ligand expression (Upd ligands are Notch direct targets; this study; (Djiane et
473 al., 2013)), and Pdp1 expression.
474 Even though Pdp1 downregulation could suppress NS neoplastic growth, it was not as
475 efficient as JNK inhibition, or Yki downregulation, suggesting that other factors in
476 parallel to Pdp1 might be involved, such as the previously identified Atf3 (Donohoe et
477 al., 2018), but also the other Notch direct target Ets21C (Fig. 2D; (Külshammer et al.,
478 2015; Toggweiler et al., 2016). This action of both Pdp1 and Ets21C suggest a
479 feedforward loop downstream of Notch that in the context of polarity loss and JNK
480 activity promotes neoplastic growth (Fig. 4G). However, since *Atf3, Pdp1*, and *Ets21C*
481 are all upregulated in N hyperplastic conditions, their sole upregulation cannot be
482 sufficient for neoplasia. The fact that Atf3 and Pdp1 iRegulon enrichments are not
483 found in N (Fig. 3 and S3), could indicate that despite being upregulated in hyperplastic
484 N, their transcriptional activities are hindered. Further studies are thus required to test
485 this possibility and study how, in the context of normal epithelial polarity, Notch
486 activation prevents the action of the Pdp1/Ets21C/Atf3 node, thus preventing the
487 transition to neoplasia.
488

489 **MATERIALS AND METHODS**

490 ***Drosophila genetics***

491 The different overgrowth paradigms were obtained by generating random clones in 3rd
492 instar wing discs at high frequency as previously published in (Djiane et al., 2013). In
493 brief, the *abxUbxFLPase; Act>y>Gal4, UAS GFP; FRT82B tubGal80* flies were
494 crossed either to *FRT82B* (to generate Ctrl discs), or to *UAS-Nicd; FRT82B* (to generate
495 hyperplastic N discs), or to *UAS-Nicd; FRT82B scrib1* (to generate neoplastic NS
496 discs). *scrib1* represents a loss of function allele for the *scribble* gene. Because *scrib1*
497 clones are eliminated in growing discs, the dysplasic S discs were obtained from
498 *FRT82B scrib1 / Df(3R)BSC752* 3rd instar larvae. All crosses were performed at 25°C
499 and carefully staged (time after egg laying and tube crowding).

500 For functional studies, neoplastic growth was obtained by driving *UAS-Nicd* and the
501 *scrib* RNAi *P{TRiP.HMS01490}attP2* by the *Bx-Gal4* (pouch of larval wing discs).
502 Modifications of the overgrowth phenotype and of the expression of the Mmp1 invasive
503 marker were performed by crossing in F1 *Bx-Gal4, UAS GFP;; UAS Nicd, UAS*
504 *scribHMS01490* to the desired *UAS RNAi* or control lines (*UAS white RNAi, UAS*
505 *yellow RNAi,* or *UAS GFP*), to ensure similar UAS load. List of lines tested in
506 Supplemental Materials.

507 Information on gene models and functions, and on *Drosophila* lines available were
508 obtained from FlyBase (flybase.org – (Thurmond et al., 2019)).

509

510 ***RNA extraction and RNA-Seq***

511 RNA from 60 or 80 dissected third instar larva wing discs of WT, N, NS and S discs
512 was extracted using TriZOL. Genomic DNA was eliminated using Ambion's DNA-
513 free kit (#AM1906). cDNA bank preparation were then performed from 1µg of RNA
514 and sequencing on a Illumina HisSeq 2000 by the Biocampus genomic facility MGX
515 of Montpellier. After sequencing, reads obtained were filtered based on their quality
516 (circa 40 millions reads were kept per conditions). The reads were then align on
517 *Drosophila* dm6 genome by the ABIC facility in Montpellier producing a matrix of
518 reads per gene and per condition. This matrix was then normalized and pair-wise
519 differential expression was performed using DESeq (Anders and Huber, 2010). Other
520 differential expression tools were tested such as DESeq2 and edgeR with default
521 parameters but appeared either less stringent, or inadequate.

522

523 ***qPCR***

524 qPCR was performed on biological triplicates on a Roche LightCycler 480, and fold
525 change was estimated by the δδCT approach. List of primers used in Supplemental
526 Materials.

527

528 ***Su(H) Chromatin Immuno Precipitation***

529 After dissection in PBS 1X, Protein/DNA complexes from 60 wing discs (80 for S
530 condition) were cross-linked with 1% formaldehyde for 10 minutes. The reaction was
531 then quenched by 0.125 M Glycine and washed 3x in PBS. Wing disc cells were
532 resuspended in 50µL Nuclear Lysis Buffer (Tris-HCl pH 8.1 20mM, EDTA 10mM,
533 SDS 1%). Lysates were sonicated on a Bioruptor (Diagenode), and diluted 10x in
534 Immunoprecipitation Dilution Buffer (Tris-HCl pH 8.1 20mM, EDTA 2mM, SDS
535 0.01%, NaCl 150mM, Triton X-100 1%) and precleared with rabbit IgG (Sigma) and
536 protein G Agarose (Santa Cruz Biotechnology). ChIP reactions were performed by
537 incubating lysates overnight at 4°C with 1ng of Goat anti-Su(H) (Santa Cruz
538 Biotechnology, sc15813), and immunocomplexes were then isolated with Protein G
539 Agarose for 2h, washed 2x with Wash Buffer 1 (Tris-HCl pH 8.1 20mM, EDTA 2mM,
540 SDS 0.1%, NaCl 50mM, Triton X-100 1%) and 2x with Wash Buffer 2 (Tris-HCl pH
541 8.1 10mM, EDTA 1mM, LiCl 250mM, NP-40 1%, Deoxycholic acid 0.4%), before a
542 decross-linking step at 65°C in 0.25M NaCl. Samples were then treated with 0.2 mg/mL
543 proteinase K and 50mg/mL RNase A. The DNA was then purified on columns (Qiagen,
544 28106). ChIP efficiency was checked by qPCR normalized on input chromatin with the
545 following primer couples, corresponding to known strong binding sites of Su(H). List
546 of primers used in Supplemental Materials.

547 For whole-genome analysis, 1 µg double-stranded ChIP or input DNA (corresponding
548 to 180 discs for each replicate) was labelled with either Cy3- or Cy5-random primers
549 using the Nimblegen Dual Colour kit. Both ChIP and input were co-hybridised to
550 NimbleGen D. melanogaster ChIP-chip 2.1 M whole-genome tiling arrays in the
551 NimbleGen hybridisation station at 42°C for 16 h and then washed according to the
552 NimbleGen Wash Buffer kit instructions. The data obtained were normalized using
553 quantile normalization across the replicate arrays in R. Window smoothing and peak
554 calling were performed using the Bioconductor package Ringo (Toedling et al., 2007)

555 with a winHalfSize of 300 bp and min.probes = 5. Probe levels were then assigned P-
556 values based on the normalNull method, corrected for multiple testing using the
557 Hochberg–Benjamini algorithm and then condensed into regions using distCutOff of
558 200 bp.
559 In order to determine the Notch Direct Targets (NDTs), ChIP and RNA-Seq results
560 were compared: NDTs are defined as up-regulated genes with Su(H) enrichment within
561 20kb. As such one Su(H) peak could be assigned to several upregulated genes
562 consistent with its role in enhancer regions. The 20kb window was chosen as it allowed
563 the recovery of more than 85% of NDTs in our previous study that was based on closest
564 gene assignment irrespective of distance (Djiane et al., 2013).
565
566 ***GO Term analyses***
567 The lists of significantly regulated genes in the various comparisons were submitted to
568 gene ontology (GO) term enrichment analysis. We used the GO biological process
569 (GOBP) ontology and applied hypergeometric tests (p-values) followed by Benjamini-
570 Hochberg multiple hypothesis correction (q-values).
571
572 ***iRegulon analyses***
573 In order to determine the likely transcriptional modules in our transcriptomic and NDTs
574 datasets, we used the online tool iRegulon (http://iregulon.aertslab.org/), with the
575 standard settings using the 6K Motif collection (6383 PWMs) and a Putative regulatory
576 region of "10kb upstream, full transcript and 10kb downstream". Importantly, these
577 settings allowed the recovery of the "positive control" Su(H) module.
578
579 ***Immunofluorescence***
580 Antibody staining of wing imaginal discs were performed using standard protocols.
581 Briefly, larval heads containing the imaginal discs (LH) were dissected in cold PBS and
582 fixed for 20min in 4% Formaldehyde in PBS at room temperature (RT), before being
583 rinsed 3x 10min in PBS 0.2% TritonX100 (PBT), and blocked in PBT + 0.5% BSA
584 (PBTB) for 30min at RT. LH were then incubated overnight at 4°C with primary
585 antibodies in PBTB. LH were then rinsed 3x 10min in PBT at RT and before being
586 incubated with secondary antibody in PBTB for 90min at RT. LH were then rinsed 3x
587 20min in PBT at RT, before being equilibrated overnight in Citifluor mounting media

588 (Agar). Discs were then further dissected and mounted. Images were acquired on a
589 Zeiss Apotome2 or Leica Thunder microscope and processed and quantified using Zen,
590 Las X, or ImageJ. Primary antibodies used were rabbit anti cleaved Drosophila Dcp-1
591 (9578, Cell Signaling Technologies, 1:200), rat anti-DE-Cadherin (DCAD2,
592 Developmental Studies Hybridoma Bank – DHSB, 1:25), rabbit anti-GFP (A6455,
593 Molecular Probes, 1:200), and mouse anti-Mmp1 (3A6B4, DHSB, 1:25). Secondary
594 antibodies used conjugated to Alexa-350, Alexa-488, or Cy3 were from Jackson Labs
595 Immuno Research (1:200).
596
597 ***Quantification methods***
598 Genotypes were tested in batches with controls and 10-20 images corresponding to 10-
599 20 different discs were all acquired on the same microscope with the same exposure
600 settings.
601 Growth was estimated by the size of the GFP positive area measured as pixel numbers.
602 Mmp1 intensities were ranked as High, Low, Null by independent observer with
603 genotypes masked and processed in random order. Graphs and statistics (indicated in
604 the legends) were performed using the GraphPad Prism software.
605

606 **ACKNOWLEDGEMENTS**
607 We thank G. Alvès, D. Andrew, D. Eberl, P. Léopold, R. Levayer, C. Maurange, A.
608 Teleman, J. Terman, and T.T. Su for sharing flies. We acknowledge the Bloomington
609 Stock Center, the Vienna Stock Center, the DGRC Kyoto Stock Center, the
610 Developmental Studies Hybridoma Bank, the *Drosophila* facility, the MGX sequencing
611 facility (BioCampus Montpellier, CNRS, INSERM, Université de Montpellier), and
612 FlyBase for their support to our research.
613 The lab of SJB is supported by the MRC (MRC programme grant MR/L007177/1). RL
614 was supported by fellowships from "Ligue Nationale Contre le Cancer - LNCC" and
615 from "Fondation ARC pour la recherche sur le cancer". The lab of AD is supported by
616 the "Fondation ARC pour la recherche sur le cancer", "Marie Curie CIG", and "Agence
617 Nationale de la Recherche - ANR".
618
619
620 **AUTHOR CONTRIBUTIONS**
621 RL, CG, PL, DK, and AD performed experiments; RL, CG, LHM, JC, and AD analyzed
622 data; JC provided expertise for RNA-Seq; BF and SJB provided technical support and
623 expertise for ChIP; RL, SJB, and AD wrote the manuscript; AD conceived and
624 supervised the project.
625
626
627 **DECLARATION OF INTEREST**
628 The authors declare no competing interests.
629

630 **REFERENCES**

631 Anders S, Huber W. 2010. Differential expression analysis for sequence count data.
632 *Genome Biol* **11**:R106. doi:10.1186/gb-2010-11-10-r106
633 Atkins M, Potier D, Romanelli L, Jacobs J, Mach J, Hamaratoglu F, Aerts S, Halder G. 2016.
634 An Ectopic Network of Transcription Factors Regulated by Hippo Signaling
635 Drives Growth and Invasion of a Malignant Tumor Model. *Curr Biol* **26**:2101–
636 2113. doi:10.1016/j.cub.2016.06.035
637 Baeg G-H, Zhou R, Perrimon N. 2005. Genome-wide RNAi analysis of JAK/STAT signaling
638 components in Drosophila. *Genes Dev* **19**:1861–1870. doi:10.1101/gad.1320705
639 Banks L, Pim D, Thomas M. 2012. Human tumour viruses and the deregulation of cell
640 polarity in cancer. *Nat Rev Cancer* **12**:877–886. doi:10.1038/nrc3400
641 Bilder D, Schober M, Perrimon N. 2003. Integrated activity of PDZ protein complexes
642 regulates epithelial polarity. *Nat Cell Biol* **5**:53–58. doi:10.1038/ncb897
643 Bray SJ. 2016. Notch signalling in context. *Nat Rev Mol Cell Biol* **17**:722–735.
644 doi:10.1038/nrm.2016.94
645 Brumby AM, Richardson HE. 2003. scribble mutants cooperate with oncogenic Ras or
646 Notch to cause neoplastic overgrowth in Drosophila. *EMBO J* **22**:5769–5779.
647 doi:10.1093/emboj/cdg548
648 Bunker BD, Nellimoottil TT, Boileau RM, Classen AK, Bilder D. 2015. The transcriptional
649 response to tumorigenic polarity loss in Drosophila. *Elife* **4**.
650 doi:10.7554/eLife.03189
651 Coopman P, Djiane A. 2016. Adherens Junction and E-Cadherin complex regulation by
652 epithelial polarity. *Cell Mol Life Sci* **73**:3535–3553. doi:10.1007/s00018-016-
653 2260-8
654 Cordenonsi M, Zanconato F, Azzolin L, Forcato M, Rosato A, Frasson C, Inui M,
655 Montagner M, Parenti AR, Poletti A, Daidone MG, Dupont S, Basso G, Bicciato S,
656 Piccolo S. 2011. The Hippo transducer TAZ confers cancer stem cell-related
657 traits on breast cancer cells. *Cell* **147**:759–772. doi:10.1016/j.cell.2011.09.048
658 Cordero JB, Macagno JP, Stefanatos RK, Strathdee KE, Cagan RL, Vidal M. 2010.
659 Oncogenic Ras diverts a host TNF tumor suppressor activity into tumor
660 promoter. *Dev Cell* **18**:999–1011. doi:10.1016/j.devcel.2010.05.014
661 Davie K, Jacobs J, Atkins M, Potier D, Christiaens V, Halder G, Aerts S. 2015. Discovery of
662 transcription factors and regulatory regions driving in vivo tumor development
663 by ATAC-seq and FAIRE-seq open chromatin profiling. *PLoS Genet* **11**:e1004994.
664 doi:10.1371/journal.pgen.1004994
665 Djiane A, Krejci A, Bernard F, Fexova S, Millen K, Bray SJ. 2013. Dissecting the
666 mechanisms of Notch induced hyperplasia. *EMBO J* **32**:60–71.
667 doi:10.1038/emboj.2012.326
668 Djiane A, Zaessinger S, Babaoğlan AB, Bray SJ. 2014. Notch inhibits Yorkie activity in
669 Drosophila wing discs. *PLoS ONE* **9**:e106211. doi:10.1371/journal.pone.0106211
670 Doggett K, Turkel N, Willoughby LF, Ellul J, Murray MJ, Richardson HE, Brumby AM.
671 2015. BTB-Zinc Finger Oncogenes Are Required for Ras and Notch-Driven
672 Tumorigenesis in Drosophila. *PLoS ONE* **10**:e0132987.
673 doi:10.1371/journal.pone.0132987
674 Donohoe CD, Csordás G, Correia A, Jindra M, Klein C, Habermann B, Uhlirova M. 2018.
675 Atf3 links loss of epithelial polarity to defects in cell differentiation and
676 cytoarchitecture. *PLoS Genet* **14**:e1007241. doi:10.1371/journal.pgen.1007241
677 Flaherty MS, Zavadil J, Ekas LA, Bach EA. 2009. Genome-wide expression profiling in the
678 Drosophila eye reveals unexpected repression of notch signaling by the
679 JAK/STAT pathway. *Dev Dyn* **238**:2235–2253. doi:10.1002/dvdy.21989
680 Fre S, Huyghe M, Mourikis P, Robine S, Louvard D, Artavanis-Tsakonas S. 2005. Notch
681 signals control the fate of immature progenitor cells in the intestine. *Nature*
682 **435**:964–968. doi:10.1038/nature03589

683 Ho DM, Pallavi SK, Artavanis-Tsakonas S. 2015. The Notch-mediated hyperplasia
684 circuitry in Drosophila reveals a Src-JNK signaling axis. *Elife* **4**:e05996.
685 doi:10.7554/eLife.05996
686 Huang L, Muthuswamy SK. 2010. Polarity protein alterations in carcinoma: a focus on
687 emerging roles for polarity regulators. *Curr Opin Genet Dev* **20**:41–50.
688 doi:10.1016/j.gde.2009.12.001
689 Igaki T, Pagliarini RA, Xu T. 2006. Loss of cell polarity drives tumor growth and invasion
690 through JNK activation in Drosophila. *Curr Biol* **16**:1139–1146.
691 doi:10.1016/j.cub.2006.04.042
692 Igaki T, Pastor-Pareja JC, Aonuma H, Miura M, Xu T. 2009. Intrinsic tumor suppression
693 and epithelial maintenance by endocytic activation of Eiger/TNF signaling in
694 Drosophila. *Dev Cell* **16**:458–465. doi:10.1016/j.devcel.2009.01.002
695 Katheder NS, Khezri R, O'Farrell F, Schultz SW, Jain A, Rahman MM, Schink KO,
696 Theodossiou TA, Johansen T, Juhász G, Bilder D, Brech A, Stenmark H, Rusten TE.
697 2017. Microenvironmental autophagy promotes tumour growth. *Nature*
698 **541**:417–420. doi:10.1038/nature20815
699 Külshammer E, Mundorf J, Kilinc M, Frommolt P, Wagle P, Uhlirova M. 2015. Interplay
700 among Drosophila transcription factors Ets21c, Fos and Ftz-F1 drives JNK-
701 mediated tumor malignancy. *Dis Model Mech* **8**:1279–1293.
702 doi:10.1242/dmm.020719
703 Kusch T, Florens L, Macdonald WH, Swanson SK, Glaser RL, Yates JR, Abmayr SM,
704 Washburn MP, Workman JL. 2004. Acetylation by Tip60 is required for selective
705 histone variant exchange at DNA lesions. *Science* **306**:2084–2087.
706 doi:10.1126/science.1103455
707 Loubiere V, Papadopoulos GL, Szabo Q, Martinez A-M, Cavalli G. 2020. Widespread
708 activation of developmental gene expression characterized by PRC1-dependent
709 chromatin looping. *Sci Adv* **6**:eaax4001. doi:10.1126/sciadv.aax4001
710 Maraver A, Fernández-Marcos PJ, Herranz D, Muñoz-Martin M, Gomez-Lopez G,
711 Cañamero M, Mulero F, Megías D, Sanchez-Carbayo M, Shen J, Sanchez-Cespedes
712 M, Palomero T, Ferrando A, Serrano M. 2012. Therapeutic effect of γ-secretase
713 inhibition in KrasG12V-driven non-small cell lung carcinoma by derepression of
714 DUSP1 and inhibition of ERK. *Cancer Cell* **22**:222–234.
715 doi:10.1016/j.ccr.2012.06.014
716 McCaffrey LM, Montalbano J, Mihai C, Macara IG. 2012. Loss of the Par3 polarity protein
717 promotes breast tumorigenesis and metastasis. *Cancer Cell* **22**:601–614.
718 doi:10.1016/j.ccr.2012.10.003
719 Ntziachristos P, Lim JS, Sage J, Aifantis I. 2014. From fly wings to targeted cancer
720 therapies: a centennial for notch signaling. *Cancer Cell* **25**:318–334.
721 doi:10.1016/j.ccr.2014.02.018
722 Ohsawa S, Sugimura K, Takino K, Xu T, Miyawaki A, Igaki T. 2011. Elimination of
723 oncogenic neighbors by JNK-mediated engulfment in Drosophila. *Dev Cell*
724 **20**:315–328. doi:10.1016/j.devcel.2011.02.007
725 Pagliarini RA, Xu T. 2003. A genetic screen in Drosophila for metastatic behavior. *Science*
726 **302**:1227–1231. doi:10.1126/science.1088474
727 Pascual J, Jacobs J, Sansores-Garcia L, Natarajan M, Zeitlinger J, Aerts S, Halder G,
728 Hamaratoglu F. 2017. Hippo Reprograms the Transcriptional Response to Ras
729 Signaling. *Dev Cell* **42**:667-680.e4. doi:10.1016/j.devcel.2017.08.013
730 Ranganathan P, Weaver KL, Capobianco AJ. 2011. Notch signalling in solid tumours: a
731 little bit of everything but not all the time. *Nat Rev Cancer* **11**:338–351.
732 doi:10.1038/nrc3035
733 Reddy KL, Rovani MK, Wohlwill A, Katzen A, Storti RV. 2006. The Drosophila Par domain
734 protein I gene, Pdp1, is a regulator of larval growth, mitosis and endoreplication.
735 *Dev Biol* **289**:100–114. doi:10.1016/j.ydbio.2005.10.042

736 Reinke AW, Baek J, Ashenberg O, Keating AE. 2013. Networks of bZIP protein-protein
737 interactions diversified over a billion years of evolution. *Science* **340**:730–734.
738 doi:10.1126/science.1233465
739 St Johnston D, Ahringer J. 2010. Cell polarity in eggs and epithelia: parallels and
740 diversity. *Cell* **141**:757–774. doi:10.1016/j.cell.2010.05.011
741 Thurmond J, Goodman JL, Strelets VB, Attrill H, Gramates LS, Marygold SJ, Matthews BB,
742 Millburn G, Antonazzo G, Trovisco V, Kaufman TC, Calvi BR, FlyBase Consortium.
743 2019. FlyBase 2.0: the next generation. *Nucleic Acids Res* **47**:D759–D765.
744 doi:10.1093/nar/gky1003
745 Toedling J, Skylar O, Sklyar O, Krueger T, Fischer JJ, Sperling S, Huber W. 2007. Ringo--an
746 R/Bioconductor package for analyzing ChIP-chip readouts. *BMC Bioinformatics*
747 **8**:221. doi:10.1186/1471-2105-8-221
748 Toggweiler J, Willecke M, Basler K. 2016. The transcription factor Ets21C drives tumor
749 growth by cooperating with AP-1. *Sci Rep* **6**:34725. doi:10.1038/srep34725
750 Turkel N, Sahota VK, Bolden JE, Goulding KR, Doggett K, Willoughby LF, Blanco E,
751 Martin-Blanco E, Corominas M, Ellul J, Aigaki T, Richardson HE, Brumby AM.
752 2013. The BTB-zinc finger transcription factor abrupt acts as an epithelial
753 oncogene in Drosophila melanogaster through maintaining a progenitor-like cell
754 state. *PLoS Genet* **9**:e1003627. doi:10.1371/journal.pgen.1003627
755 Uhlirova M, Bohmann D. 2006. JNK- and Fos-regulated Mmp1 expression cooperates
756 with Ras to induce invasive tumors in Drosophila. *EMBO J* **25**:5294–5304.
757 doi:10.1038/sj.emboj.7601401
758 Wu M, Pastor-Pareja JC, Xu T. 2010. Interaction between Ras(V12) and scribbled clones
759 induces tumour growth and invasion. *Nature* **463**:545–548.
760 doi:10.1038/nature08702
761 Xia S, VanKuren NW, Chen C, Zhang L, Kemkemer C, Shao Y, Jia H, Lee U, Advani AS,
762 Gschwend A, Vibranovski MD, Chen S, Zhang YE, Long M. 2021. Genomic
763 analyses of new genes and their phenotypic effects reveal rapid evolution of
764 essential functions in Drosophila development. *PLoS Genet* **17**:e1009654.
765 doi:10.1371/journal.pgen.1009654
766 Xue B, Krishnamurthy K, Allred DC, Muthuswamy SK. 2013. Loss of Par3 promotes
767 breast cancer metastasis by compromising cell-cell cohesion. *Nat Cell Biol*
768 **15**:189–200. doi:10.1038/ncb2663
769
770

771 **FIGURE LEGENDS**

772 **Figure 1. Notch-based neoplastic growth paradigms in *Drosophila* wing discs**

773 **A-D.** 3rd instar wing imaginal discs at precisely 5 days after egg-laying either wild-
774 type (WT; A), overexpressing activated Notch (N; B), mutant for *scrib* (S; C), or
775 combining overexpressed Notch and *scrib* mutation (NS; D) and marked for E-Cad
776 (blue) and Mmp1 (red). **A,B&D.** MARCM clones (positively marked by GFP; green)
777 of the indicated genotypes: expressing only GFP (A; WT), expressing Nicd & GFP (B;
778 N), and expressing Nicd & GFP and mutant for *scrib* (C; NS). **C.** Discs fully mutant
779 for *scrib*.

780 **E-F.** Differentially expressed genes as compared to WT in the different growth
781 paradigms N (green), S (red), and NS (blue) identified by RNA-Seq. This color code,
782 green for N, red for S, and blue for NS is used in all figures. **E.** Heatmap of gene
783 expressions after unsupervised clustering. **F.** Venn diagram of up-regulated and down-
784 regulated genes in N, S, and NS.

785 **G.** Enrichment diagram as measured by adjusted p-value for selected GO terms and
786 represented as bars for N (green), S (red), and NS (blue). GO terms color reflect whether
787 they are shared or specific: shared by all (black), common N&NS (dark green: mix of
788 green and blue), common S&NS (purple: mix of red and blue).

789 **H.** Venn diagram showing the domains of overlap of GO terms identified (significantly
790 enriched) in N, S, and NS.

791

792 **Figure 2. Polarity loss redirects the transcriptional output of Notch during**
793 **neoplastic growth**

794 **A.** Experimental set-up to identify the Notch Direct Targets genes (NDTs): Genes up-
795 regulated in N, S, or NS (Transcriptomic), and located within 20kb of a Su(H) binding
796 site (ChIP).

797 **B.** Venn diagram showing the NDTs overlap in N, S, and NS, showing core Notch
798 responses, but also significant condition specific NDTs.

799 **C.** Overlap of the Su(H) binding sites identified by ChIP in N, S, and NS, showing that
800 almost all S and NS Su(H) peaks are also found in N. The overlap is shown in white.
801 Numbers are slightly different because in the Su(H) peaks calling protocol, in some rare
802 cases, some peaks can be split between conditions where one peak in one condition
803 would overlap with two peaks in the other.

804 **D.** Genome Viewer snapshots of several NDTs (shown in purple) such as the NS
805 specific *Act87E* and *Wnt10* (but also *yellow-e* and *Ir87a*), the common *Ets21C*, and the
806 N/NS NDT *upd3*. For each condition, the Su(H) ChIP enrichment is shown in the upper
807 lane, and the Su(H) peaks identified are represented by the blocks underneath.
808
809 **Figure 3. Identification of potential transcriptional modules mediating N, S, and**
810 **NS growth**
811 Venn diagram of significant transcription factors (TFs) identified by iRegulon as
812 potential key mediators for the expression of the N (in the green circle), S (red circle),
813 and NS (blue circle) up-regulated genes. Fed with lists of co-regulated genes, and
814 analyzing the genomic features in the vicinity of the transcription start sites of these
815 genes, iRegulon identifies potential groups of TFs and DNA-binding factors, that are
816 enriched in the dataset of regulatory sequences, and could thus represent potential
817 mediators of the N, S, and NS transcriptomes. TFs were color-coded according to their
818 molecular class and/or belonging to the similar regulon (see Supplemental table S4).
819 Numbers represent the number of TFs identified. See also Figure S3 for the iRegulon
820 analyses of the NDTs, and the detailed lists of both iRegulon analyses in Supplemental
821 Table S5.
822
823 **Figure 4. Neoplastic growth is mediated by the "oncogenic module" and by a**
824 **diverse network of bZIP transcription factors including Xrp1**
825 **A-D.** 3rd instar wing imaginal discs expressing *GFP*, an activated form of Notch (*Nicd*)
826 and an RNAi for *scrib* under the control of the *Bx-Gal4* driver (dorsal wing pouch) and
827 stained for GFP (green, white A'-D') to assess tissue overgrowth and for Mmp1 (red,
828 white A''-D'') to assess tissue invasiveness. Discs also expressed under *Bx-Gal4*
829 control the either *UAS Bsk DN* (B) or the indicated RNAi constructs: *w[HMS00045]*
830 (A; Ctrl), *yki[HMS00041]* (C), *Pdp1[HMS02030]* (D). Representative discs are shown.
831 **E.** Quantification of the overgrowth of the GFP territory in the indicated genotypes.
832 Results are shown as violin plots of total GFP area measured in arbitrary pixels. In grey
833 are represented the controls for each experiment. Statistical tests: ANOVA (left and
834 middle graphs) or unpaired t-test (right graph); n.s. non significant; * $p<0.05$; **
835 $p<0.01$; *** $p<0.001$; **** $p<0.0001$.

836 For more details of RNAi lines either from the TRiP collection (labelled with trip
837 superscript) or from the Vienna collection (labelled with KK superscript) are provided
838 in supplemental information.
839 **F.** Quantification of the Mmp1 intensity in the indicated genotypes. Results are shown
840 as percentage where discs were classified to fall in three categories: High Mmp1
841 staining intensity (red, similar to that shown in A''), Low Mmp1 staining intensity
842 (blue, similar to that shown in D''), No Mmp1 staining (light blue, similar to that shown
843 in B''). Statistical test: chi-square test for trend or Fisher's exact test; * $p<0.05$.
844 **G.** Feedforward model of the cooperation between Notch and polarity loss during wing
845 imaginal disc neoplastic growth.
846

847 **SUPPLEMENTAL INFORMATION**

848

849 **SUPPLEMENTAL MATERIAL AND METHODS**

850 ***Drosophila genetics***

851 Driver lines were *Bx-Gal4* (wing disc pouch), *Dpp-Gal4*, and *Ptc-Gal4* (both wing disc
852 antero-posterior boundary). Overexpression lines were *UAS Nicd* (made by the Bray
853 lab), *UAS GFP:Act87E [7-6]* BL#9249, and *UAS Pdp1.T* BL#78087.
854 Overexpression lines tested in the *Bx-Gal4, UAS GFP;; UAS Nicd, UAS*
855 *scribHMS01490* screen were *UAS GFP*, *UAS bskK53R [20.1a]* BL#9311, and *UAS*
856 *SOD CAT* (gift from P. Leopold). RNAi lines used are listed in the table below with an
857 indication of the labels used in Fig. 4E&F. TRiP collection lines have a stock BL#, and
858 Vienna collection lines have a stock v#. While performing the *Bx>NS* modifier
859 experiments, we used controls originating from the same collection: *RNAi white* for
860 TRiP lines, and *RNAi yellow* for Vienna KK lines.

861

Gene	RNAi ID	Stock #
Act87E	HMS02488	BL#42642
Act87E	KK111781	v#102480
cdi	KK100725	v#109409
CG7059	GD10763	v#21651
CG13850	KK104804	v#100863
CG13857	GD6226	v#44061
CG18596	KK104660	v#108183
ftz-f1	HMS00019	BL#33625
Ir87a	HMJ22848	BL#60476
Ir87a	KK106593	v#100667
kay	HMS00254	BL#33379
p53	HMS02286	BL#41720
Pdp1	HMS02030	BL#40863
Pdp1	KK109014	v#110551
REG	KK102083	v#110156
stat92E	HMS00035	BL#33637

vito	KK111866	v#102513
w	HMS00045	BL#33644
y	KK104196	v#106068
yellow-e	HMC06250	BL#65970
yellow-e	KK106243	v#100926
yellow-e3	KK106158	v#105879
yki	HMS00041	BL#34067

Primers

qPCR primers:

Act5C_F: GAGCGCGGTTACTCTTTCAC

Act5C_R: ACTTCTCCAACGAGGAGCTG

Act87E_F: GTCCACCGCAAGTGCTTCTA

Act87E_R: TTTCTTTGGATGGCAGGGCA

Atf3_F: CAGCATGGCAACATTGGGAC

Atf3_R: ATGAAGGCAGTGGCTGAGTC

Diap1_F: CAGCCACACGCATCTTCAAC

Diap1_R: ACTTTGTCACAGAGGAGGCG

E2f1_F: ACAGAATCCTCGCCTCCAAC

E2f1_R: GACTGCTGCCGTAGCCTATT

Ets21C_F: CTGCTCGCTGATTCGTCCAA

Ets21C_R: TAGGCATACCGCTTTCCGTG

ftz-f1_F: ATTCCTGGTCGGACATGCTT

ftz-f1_R: TTCATGCAGACATAGTCGCCC

mxc_F: ACTAGAGGAGGAGCAGCGAA

mxc_R: CTAGTGGACAGCGGCGTATT

p38a_F: TACGGACAGGTGTCAAAGGC

p38a_R: CAGCGATCCATTAGCGGGAT

p53_F: TGCGTGTGTTCCTTTGCTTC

p53_R: GTTCAGGGGGACTACAACGG

puc_F: ATTGACCTCGCCGCCAATTA

puc_R: ATTCCGCTTGAACAGAGCCA

888 sd_F: AGGGTCCACAGAATGCGTTT
889 sd_R: TCGCTTTCCACCTTCTCCAC
890 Sdr_F: CGCTCCCTCAATCCCAAAGT
891 Sdr_R: ACAACGTCCATCAGCCAGTT
892 Ser_F: GCACGAATCTCTGGTGTGGA
893 Ser_R: TAGATTTGGCTGGCAGTCGG
894 wg_F: GCAGTCTGGTCTGGTCTACG
895 wg_R: ATTGTGCGGGTTCAGTTGGA
896 Wnt10_F: AATGGCATCGGTGGAACTGT
897 Wnt10_R: CAGCGTCTTGCGATTGATGG
898
899 qChIP primers:
900 E(spl)mβ_F: AAGTCGGAGCTTTGAATGAG
901 E(spl)mβ_R: CAAGTCATTTTATTGCCCTCAC
902 E(spl)m5_F: GTTTCCGCAGGTCCAGTTAC
903 E(spl)m5_R: GTTTGATGTTCACGCTGCTG
904 white_F: CGAAGGACGTTGACACATTG
905 white_R: GAATTGCCGCTTTTTCTCAC
906 DDC_F: AAGTGGGATTTGCCAGTGAC
907 DDC_R: TGCTGGTGAACTTTGACTGC
908 CG42808_F: CTCGTTAAGAGCAACTGCGA
909 CG42808_R: GTGAGAACTCCGAATCGAGG
910 CG6191_F: CGAAAAATGCGGACGATTCC
911 CG6191_R: CCCACCAATCTAGGGTTTCA
912 Ilp8_F: TCATCTCCGGTGTCTGACTT
913 Ilp8_R: AAAGAATTGGCTGCGGAAGA
914
915
916 **SUPPLEMENTAL FIGURE LEGENDS**
917 **Figure S1. Features of the Notch Direct Targets (NDTs) in N, S, and NS (relates to**
918 **Fig. 3)**
919 **A.** Semi-quantitative RT-PCR of the indicated genes represented as fold change
920 compared to WT (grey) in the different N (green), S (red), and NS (blue) growth

921 paradigms and normalized to *Atc5C* expression. Biological triplicates, standard error to
922 the mean (s.e.m.) is shown.
923 **B.** Heatmaps for the expression of the different NDTs in WT, N, S, and NS. From left
924 to right are presented the N, S, NS, and finally All NDTs, highlighting that NDTs could
925 be transcriptionally up-regulated in more than in one condition.
926 **C.** Genome browser view of the whole left arm of the 2nd chromosome, and showing
927 the Su(H) ChIP enrichment (upper rows) and the intervals called as Su(H) peaks (lower
928 rows) in N (green), NS (blue), and S (red). Note the higher number of peaks in N, and
929 the rarity of NS, or S peaks not found in N.
930
931 **Figure S2. Act87E promotes Mmp1 expression and cell delamination.**
932 **A-B.** GFP:Act87E overexpressed together with activated Notch (Nicd) under the
933 control of the *Ptc-Gal4* driver (antero/posterior boundary cells in green, A'&B'),
934 promotes the expression of the Dcp-1 caspase (red, A''), and the metalloprotease Mmp1
935 (red, B''). Similar results were obtained for the sole overexpression of GFP:Act87E
936 (without Nicd). DAPI (blue, A''') or E-Cad (blue, B''') mark all wing disc cells. (A)
937 Whole wing disc. (B) Detail of the overgrowing wing pouch (magnification in B is
938 twice that in A).
939
940
941 **Figure S3. Identification of potential transcriptional modules mediating N, S, and**
942 **NS growth (relates to Fig. 3)**
943 Venn diagram of significant transcription factors identified by iRegulon in N, S, and
944 NS Notch Direct Targets, and color-coded according to their molecular class. Numbers
945 represent the number of transcription factors identified in each group. See also the
946 detailed lists of iRegulon analyses in Supplemental tables S4&5.
947
948 **Figure S4. Pdp1 is a direct Notch target (relates to Fig. 4)**
949 **A.** Genome browser view of the *Pdp1* locus, and showing the Su(H) ChIP enrichment
950 (upper rows) and the intervals called as Su(H) peaks (lower rows) in N (green), NS
951 (blue), and S (red).
952 **B-C.** Pdp1 overexpression causes cell delamination. GFP alone (B) or in combination
953 with Pdp1 (C) was overexpressed using the *Dpp-Gal4* driver. GFP is shown in green

954 (B'&C'). E-Cad is shown in blue (B''&C''). Pdp1 overexpression results in folded
955 discs (yellow arrowhead), indicative of cell delamination: note the broader patchy GFP
956 stripe upon Pdp1 overexpression.
957
958 **SUPPLEMENTAL TABLES**
959 **Table S1.** Differentially expressed genes in N, S, and NS identified by DESeq (related
960 to Fig. 1). Columns are:
961 FBgn_ID: Unique FlyBase gene ID
962 Symbol: Current FlyBase gene symbol
963 qval: adjusted p-value for multiple testing
964 logFC: log2 of the Fold Change "Condition N, S, or NS" / "Control WT"
965
966
967 **Table S2.** Su(H) ChIP enrichment peaks coordinates in N, S, and NS (related to Fig.
968 3). Columns are:
969 Exp: N, S, or NS
970 Chr: Chromosome arm
971 MIN: smallest peak coordinate
972 MAX: biggest peak coordinate
973
974
975 **Table S3.** All Notch Direct Targets (NDTs) ordered by genomic position. This table
976 includes an indication whether the genes are transcriptionally upregulated or have a
977 Su(H) peak in the vicinity in each N, S, and NS condition. Columns are:
978 N/NS/S: NDT in the corresponding condition
979 Type: NDT in different conditions.
980 FBgn_ID: Unique FlyBase gene ID
981 SYMBOL: Current FlyBase gene symbol
982 K_ARM: Chromosome arm location of the gene
983 MIN (gene pos): smallest gene coordinate
984 MAX (gene pos): biggest gene coordinate
985 STRAND: +1 or -1
986 N Fold: Log2 Fold Change in gene expression N/WT (n.s. not significant)

987 N ChIP: Su(H) ChIP enrichment peak within 20kb in N (green yes, red no)
988 NS Fold: Log2 Fold Change in gene expression NS/WT (n.s. not significant)
989 NS ChIP: Su(H) ChIP enrichment peak within 20kb in NS (green yes, red no)
990 S Fold: Log2 Fold Change in gene expression S/WT (n.s. not significant)
991 S ChIP: Su(H) ChIP enrichment peak within 20kb in S (green yes, red no)
992
993 **Table S4.** Curated iRegulon analyses of the significantly upregulated genes in N, S,
994 and NS (related to Fig. 3). Analyses were performed using the 6K-PWM and 10kb
995 upstream and downstream set-ups.
996
997 **Table S5.** Curated iRegulon analyses of the Notch Direct Targets in N, S, and NS
998 (related to Fig. S2). Analyses were performed using the 6K-PWM and 10kb upstream
999 and downstream set-ups.
1000

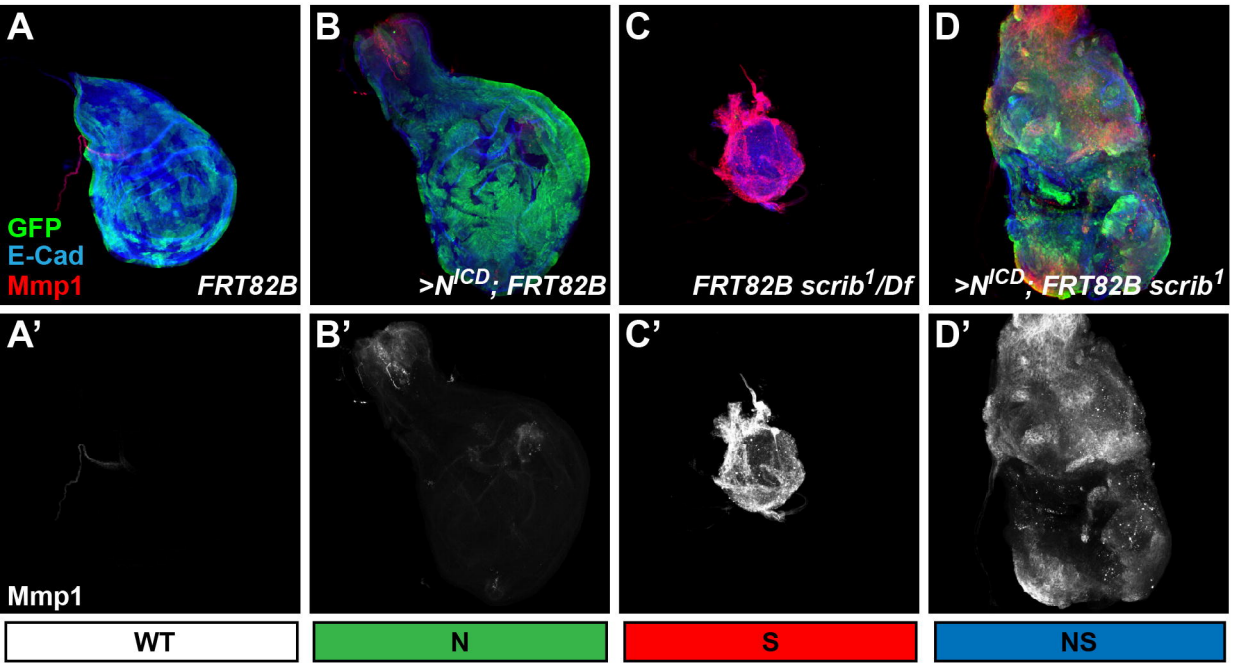
A
GFP
E-Cad
Mmp1
FRT82B
B
>N^ICD; FRT82B
C
FRT82B scrib1/Df
D
>N^ICD; FRT82B scrib1
A'
B'
C'
D'
Mmp1
WT
N
S
NS

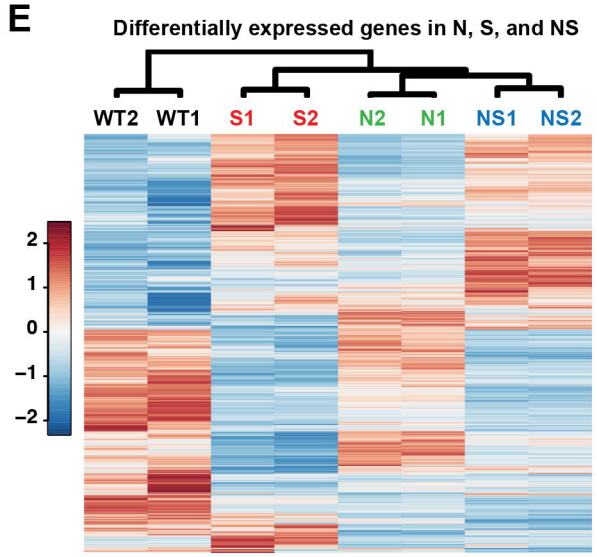
E
Differentially expressed genes in N, S, and NS
WT2
WT1
S1
S2
N2
N1
NS1
NS2
2
1
0
−1
−2

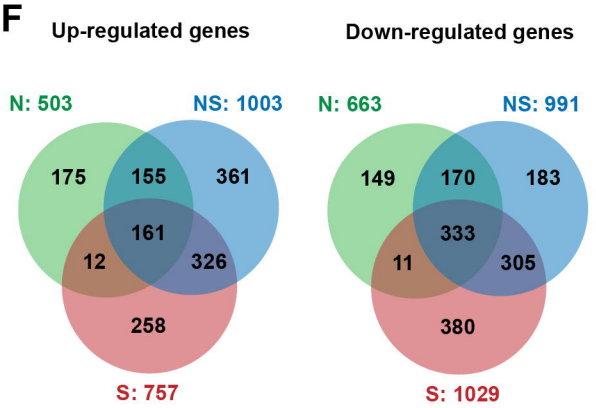
F
Up-regulated genes
N: 503
NS: 1003
175
155
361
161
12
326
258
S: 757
Down-regulated genes
N: 663
NS: 991
149
170
183
333
11
305
380
S: 1029

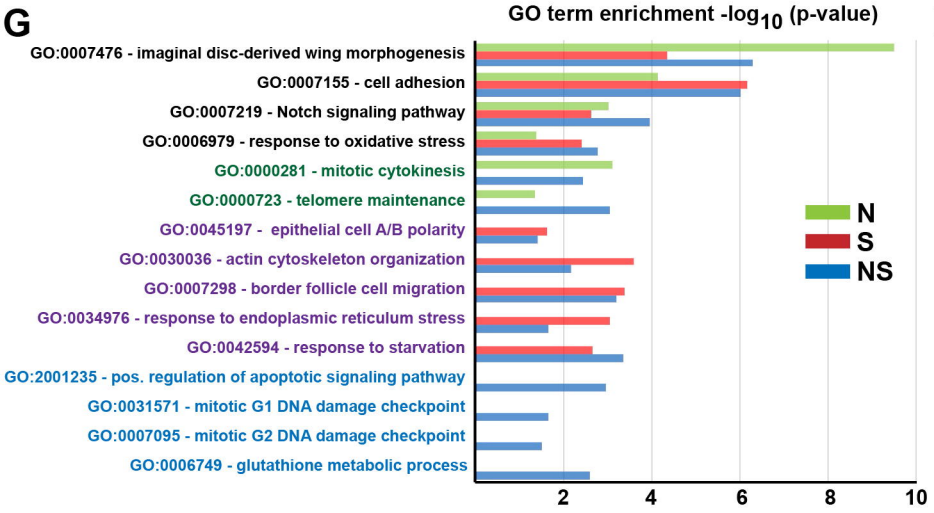
G
GO term enrichment -log10 (p-value)
GO:0007476 - imaginal disc-derived wing morphogenesis
GO:0007155 - cell adhesion
GO:0007219 - Notch signaling pathway
GO:0006979 - response to oxidative stress
GO:0000281 - mitotic cytokinesis
GO:0000723 - telomere maintenance
GO:0045197 - epithelial cell A/B polarity
GO:0030036 - actin cytoskeleton organization
GO:0007298 - border follicle cell migration
GO:0034976 - response to endoplasmic reticulum stress
GO:0042594 - response to starvation
GO:2001235 - pos. regulation of apoptotic signaling pathway
GO:0031571 - mitotic G1 DNA damage checkpoint
GO:0007095 - mitotic G2 DNA damage checkpoint
GO:0006749 - glutathione metabolic process
N
S
NS
2
4
6
8
10

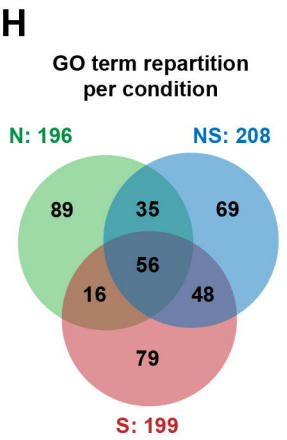
H
GO term repartition per condition
N: 196
NS: 208
89
35
69
56
16
48
79
S: 199

Logeay et al. Figure 2

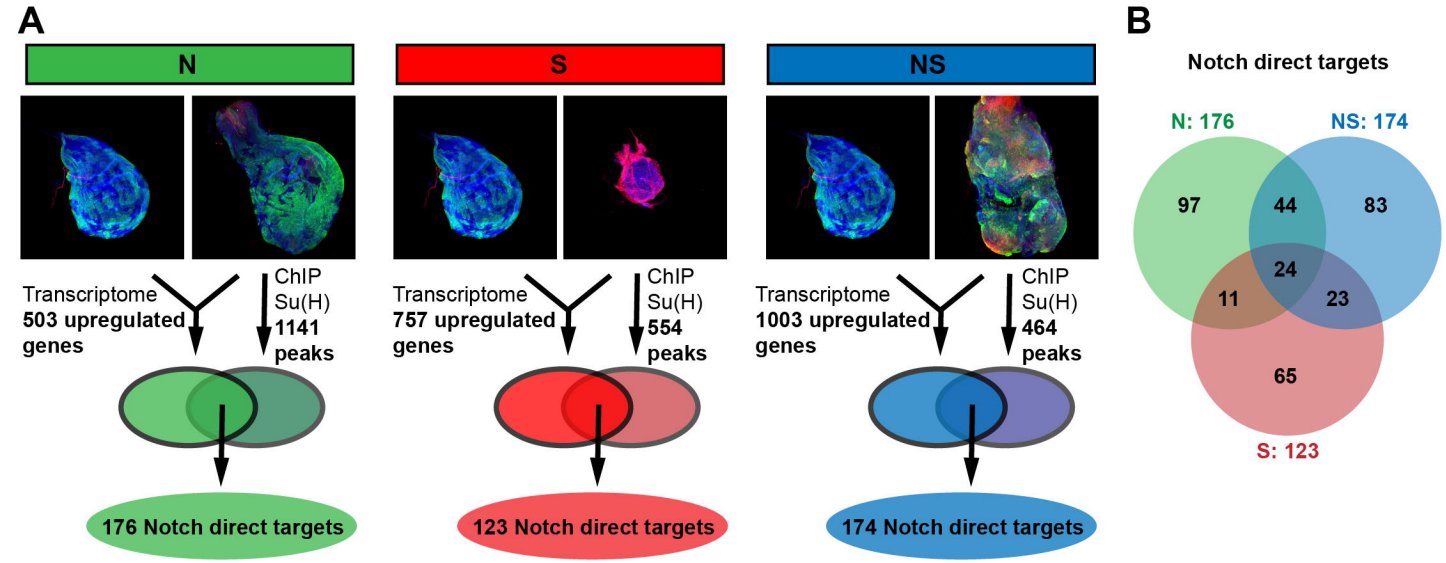

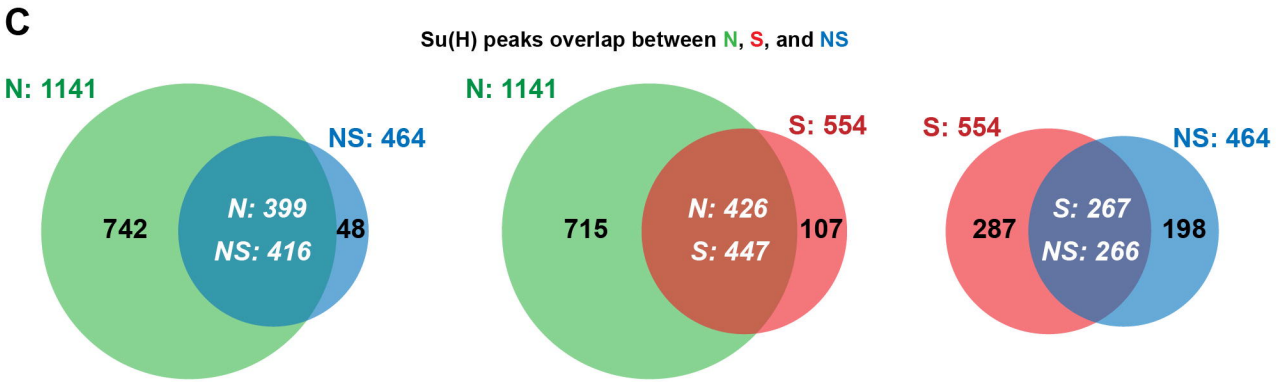

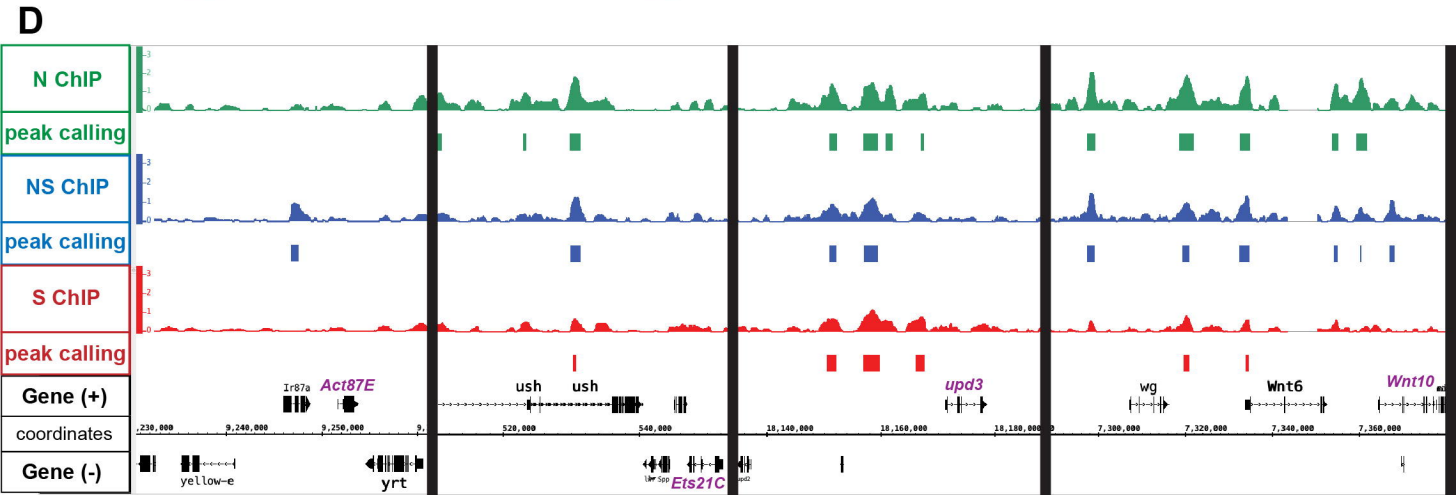

Logeay et al. Figure 3

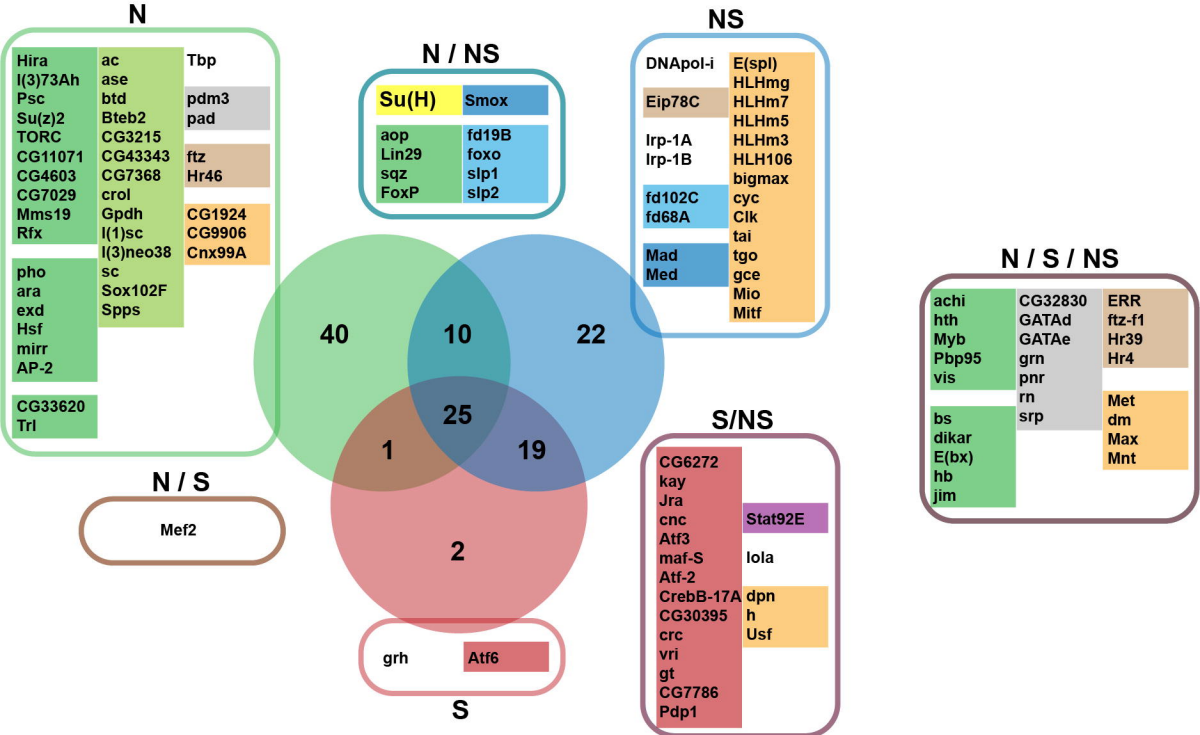

Logeay et al. Figure 4

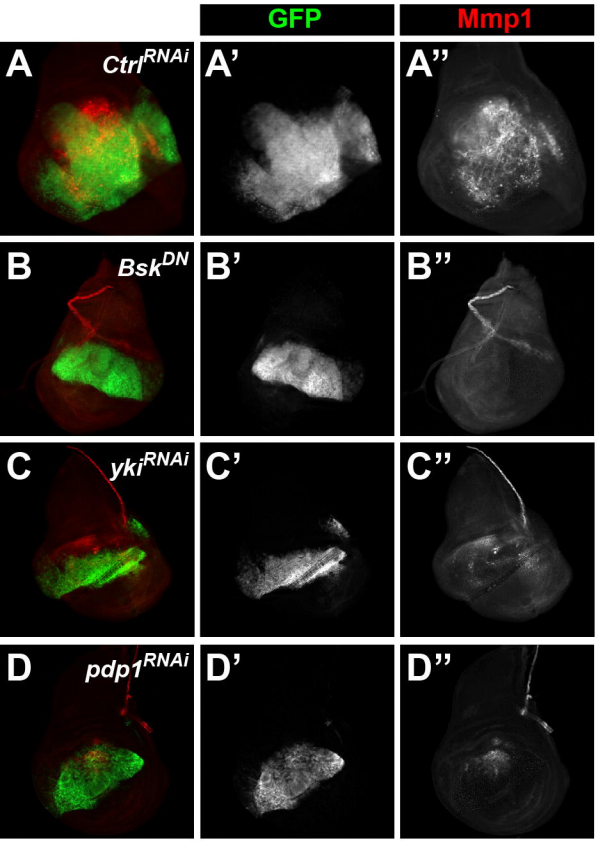

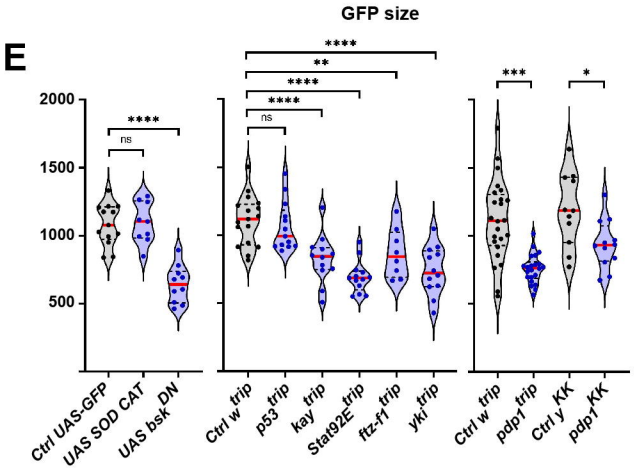

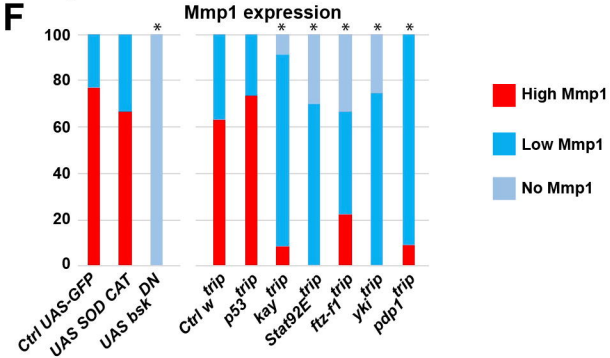

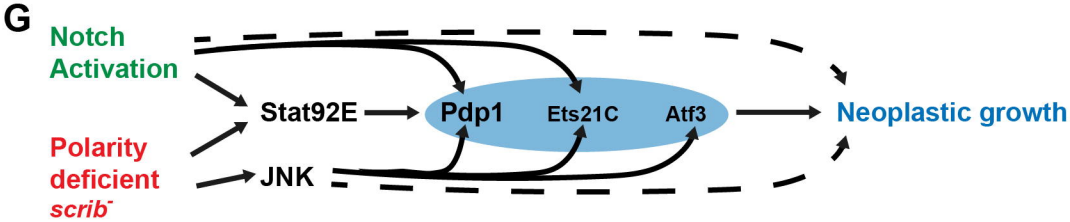

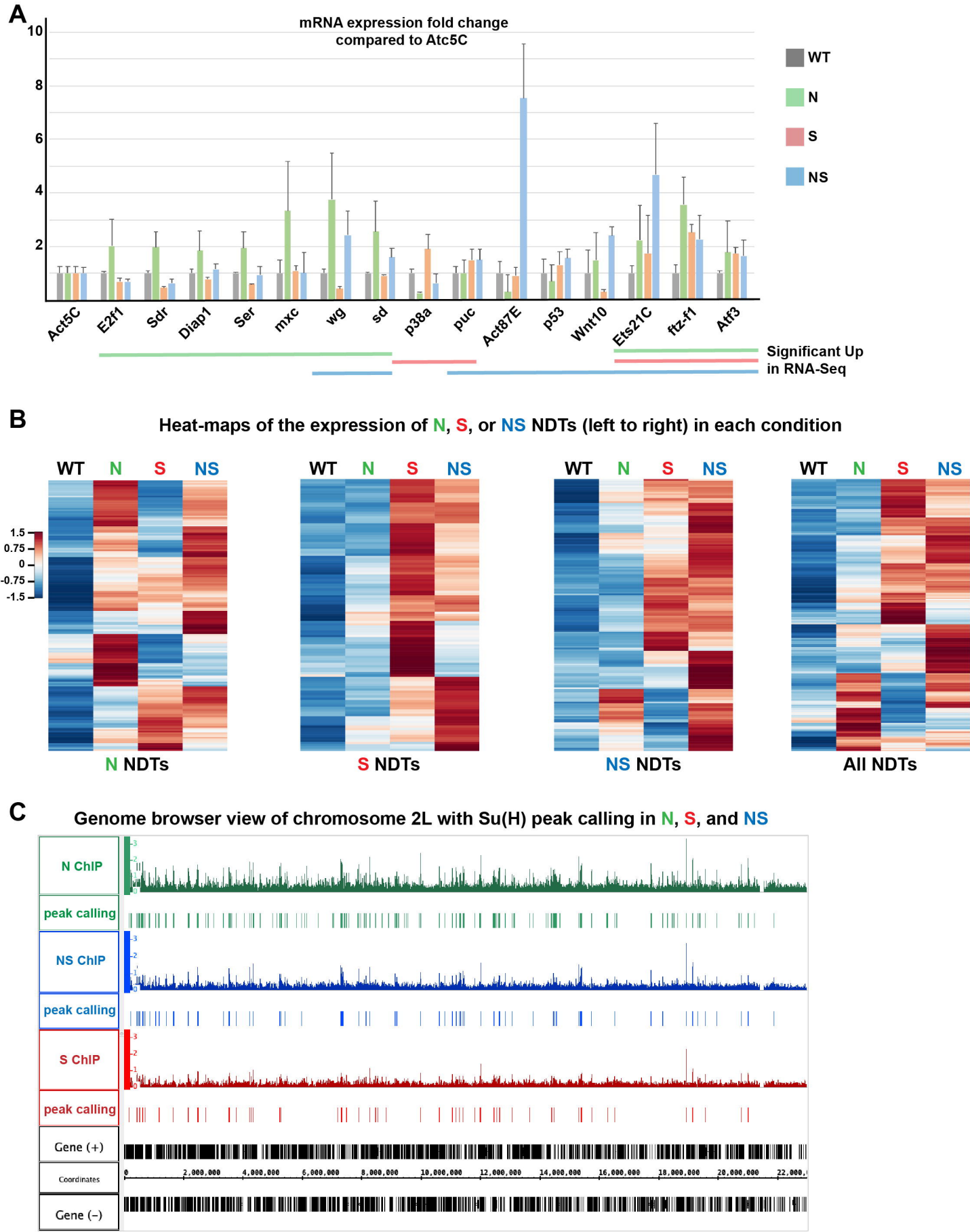
A
mRNA expression fold change compared to Atc5C
10
8
6
4
2
WT
N
S
NS
Act5C
E2f1
Sdr
Diap1
Ser
mxc
wg
sd
p38a
puc
Act87E
p53
Wnt10
Ets21C
ftz-f1
Atf3
Significant Up in RNA-Seq
B
Heat-maps of the expression of N, S, or NS NDTs (left to right) in each condition
WT N S NS
1.5
0.75
0
-0.75
-1.5
N NDTs
S NDTs
NS NDTs
All NDTs
C
Genome browser view of chromosome 2L with Su(H) peak calling in N, S, and NS
N ChIP
peak calling
NS ChIP
peak calling
S ChIP
peak calling
Gene (+)
Coordinates
Gene (–)
0
2,000,000
4,000,000
6,000,000
8,000,000
10,000,000
12,000,000
14,000,000
16,000,000
18,000,000
20,000,000
22,000,

Logeay et al. Figure S2

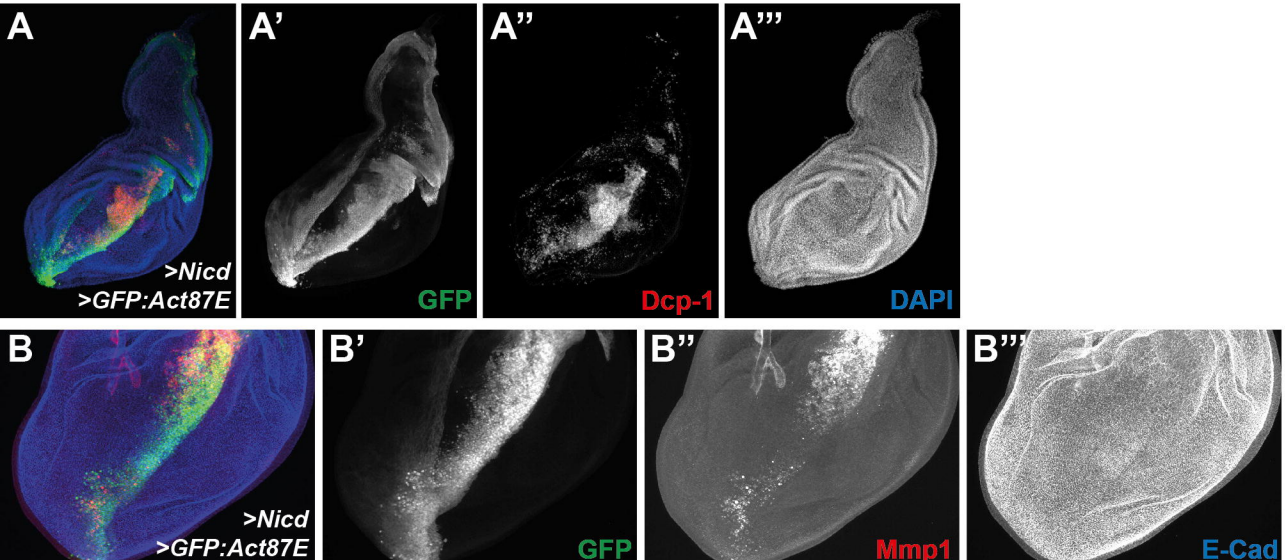

Logeay et al. Figure S3

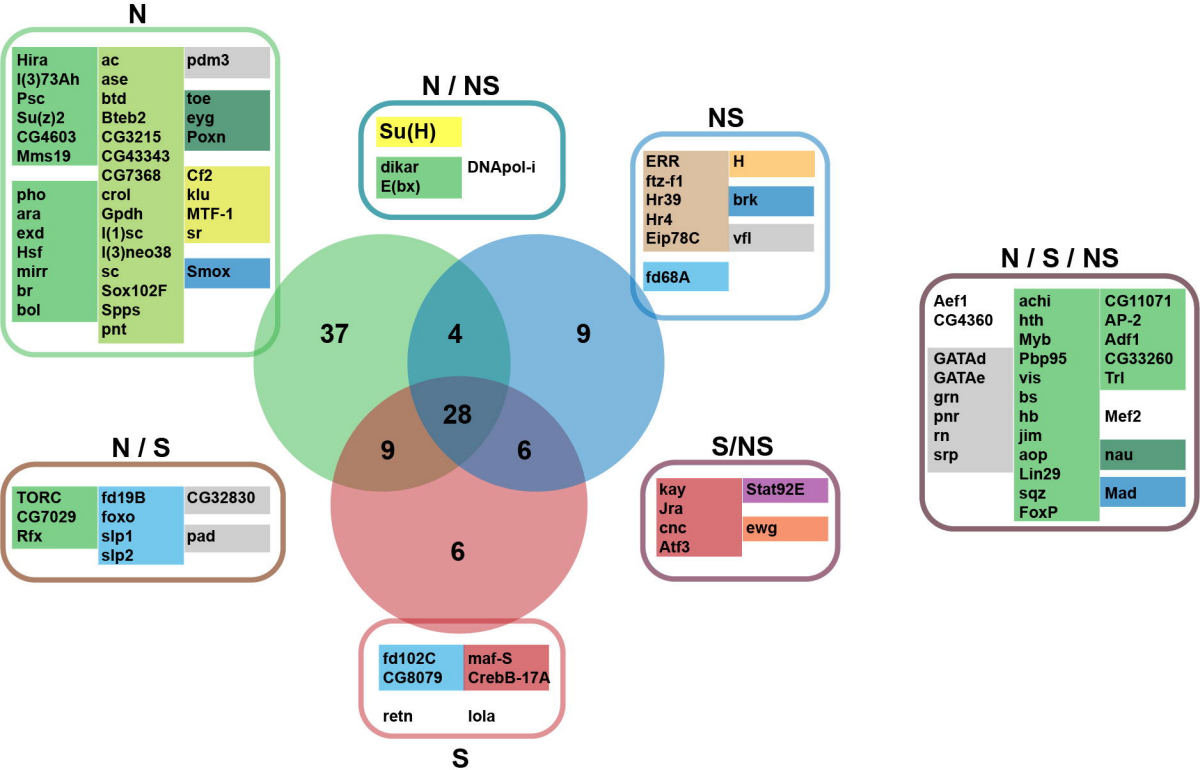
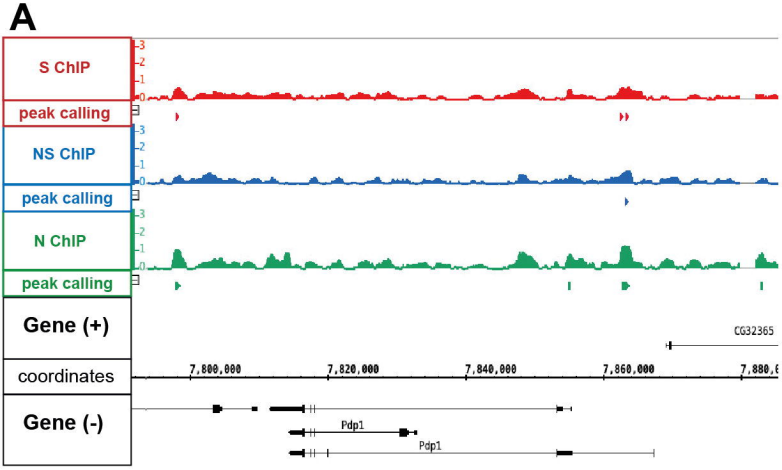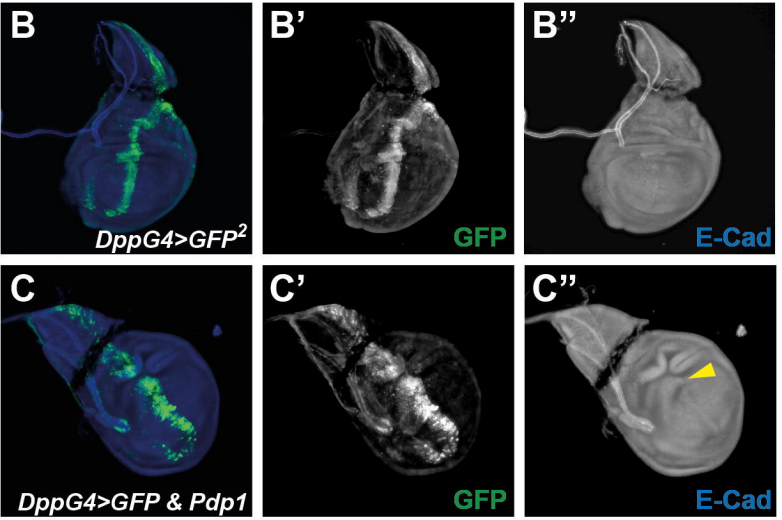
Logeay et al. Figure S4